SJSU SAN JOSÉ STATE UNIVERSITY

MTI MINETA TRANSPORTATION INSTITUTE

Sensitivity Analysis of the IDEAL CT Test Using the Distinct Element Method

Shadi Saadeh, PhD

Maria El Asmar

CSUTC California State University Transportation Consortium

CALIFORNIA STATE UNIVERSITY LONG BEACH

CSU TRANSPORTATION CONSORTIUM

transweb.sjsu.edu/csutc

Mineta Transportation Institute

Founded in 1991, the Mineta Transportation Institute (MTI), an organized research and training unit in partnership with the Lucas College and Graduate School of Business at San José State University (SJSU), increases mobility for all by improving the safety, efficiency, accessibility, and convenience of our nation's transportation system. Through research, education, workforce development, and technology transfer, we help create a connected world. MTI leads the Mineta Consortium for Transportation Mobility (MCTM) funded by the U.S. Department of Transportation and the California State University Transportation Consortium (CSUTC) funded by the State of California through Senate Bill 1. MTI focuses on three primary responsibilities:

Research

MTI conducts multi-disciplinary research focused on surface transportation that contributes to effective decision making. Research areas include: active transportation; planning and policy; security and counterterrorism; sustainable transportation and land use; transit and passenger rail; transportation engineering; transportation finance; transportation technology; and workforce and labor. MTI research publications undergo expert peer review to ensure the quality of the research.

Education and Workforce

To ensure the efficient movement of people and products, we must prepare a new cohort of transportation professionals who are ready to lead a more diverse, inclusive, and equitable transportation industry. To help achieve this, MTI sponsors a suite of workforce development and education opportunities. The Institute supports educational programs offered by the Lucas Graduate School of Business: a Master of Science in Transportation Management, plus graduate certificates that include High-Speed and Intercity Rail Management and Transportation Security Management. These flexible programs offer live online classes so that working transportation professionals can pursue an advanced degree regardless of their location.

Information and Technology Transfer

MTI utilizes a diverse array of dissemination methods and media to ensure research results reach those responsible for managing change. These methods include publication, seminars, workshops, websites, social media, webinars, and other technology transfer mechanisms. Additionally, MTI promotes the availability of completed research to professional organizations and works to integrate the research findings into the graduate education program. MTI's extensive collection of transportation-related publications is integrated into San José State University's world-class Martin Luther King, Jr. Library.

Report 23-22

Sensitivity Analysis of the IDEAL CT Test Using the Distinct Element Method

Shadi Saadeh, PhD

Maria El Asmar

September 2023

A publication of the
Mineta Transportation Institute
Created by Congress in 1991
College of Business
San José State University
San José, CA 95192-0219

TECHNICAL REPORT DOCUMENTATION PAGE

1. Report No 23-22	**2. Government Accession No.**	**3. Recipient's Catalog No.**	
4. Title and Subtitle Sensitivity Analysis of the IDEAL CT Test Using the Distinct Element Method		**5. Report Date** September 2023	
		6. Performing Organization Code	
7. Authors Shadi Saadeh, PhD Maria El Asmar		**8. Performing Organization Report** CA-MTI-2243	
9. Performing Organization Name and Address Mineta Transportation Institute College of Business San José State University San José, CA 95192-0219		**10. Work Unit No.**	
		11. Contract or Grant No. ZSB12017-SJAUX	
12. Sponsoring Agency Name and Address State of California SB1 2017/2018 Trustees of the California State University Sponsored Programs Administration 401 Golden Shore, 5th Floor Long Beach, CA 90802		**13. Type of Report and Period Covered**	
		14. Sponsoring Agency Code	
15. Supplemental Notes			

16. Abstract

Cracking is a primary mode of failure for asphalt concrete (AC), resulting in road damage and deterioration, and leading to an increase in road hazards and fatalities. Studying the fracture behavior of AC is an effective way to learn how to best enhance their cracking resistance. To do this, the indirect tensile cracking laboratory test (IDEAL-CT) was developed and used to assess the AC cracking behavior by defining a unique index that allows the ranking of different mixes' cracking resistance. The sensitivity of the test results to the test parameters is needed to monitor the test's performance. Several parameters impact the result of the IDEAL-CT. This study focuses on the variation of air voids, loading rate, aggregate shape, bonding type, and gradation mix. Performing more than 450 test scenarios—varying multiple factors and conducting enough tests for each variation—would require considerable resources and time. To solve the issue, the Particle Flow Code in two-dimension software (PFC2D) using the discrete element method (DEM) is adapted to mitigate the need for actual laboratory tests. Initial findings yielded a better understanding of the micromechanical behavior of each mix, showing that air void content has more impact than loading rate; a decrease of 2% in air voids resulted in an increase of more than 50% in cracking resistance. Additionally, different aggregate sources and bonding strengths affected the cracking resistance. These results can inform further studies on AC cracking in order to reduce road damage and deterioration to keep roads safe.

17. Key Words CT-Index, DEM, Asphalt mixture, Air voids, Loading rate, Aggregate shape, and Bonding type	**18. Distribution Statement** No restrictions. This document is available to the public through The National Technical Information Service, Springfield, VA 22161.		
19. Security Classif. (of this report) Unclassified	**20. Security Classif. (of this page)** Unclassified	**21. No. of Pages** 79	**22. Price**

Form DOT F 1700.7 (8-72)

DOI: 10.31979/mti.2243

Mineta Transportation Institute
College of Business
San José State University
San José, CA 95192-0219

Tel: (408) 924-7560
Email: mineta-institute@sjsu.edu
transweb.sjsu.edu/research/2243

Acknowledgments

The authors would like to thank the State of California and the California State University Transportation Consortium for their contribution to fund this project.

CONTENTS

List of Figures

List of Tables

1. Introduction

Fatigue cracking is one of the major pavement distresses caused by an increase in traffic volume. One often-heard complaint is that recent pavement mixes are more susceptible to cracking, and the need to enhance cracking resistance has increasingly been a major focus for engineers. A longstanding primary goal of the study of asphalt concrete has been to obtain the most economic mix with adequate cracking resistance under a repetitive load. Aggregates represent the skeleton of the mix; their source, shape, and texture influence mix performance, while air voids ensure the durability and permeability of the mix, and the percentage of air voids also influences the mix's resistance to cracking. Finally, the asphalt glues the components together. However, asphalt is a highly viscous material and behaves differently under different loads, which affect its volume, air voids' percentage, and source influence, as well as its performance. Throughout this study, a literature review is conducted, followed by a methodology section explaining the software modelling applied for the IDEAL-CT, then the results are discussed in the analysis section.

Multiple cracking tests were adapted to assess cracking resistance, such as the Texas OT test, the semi-circular bending test (SCB), and the IDEAL-CT (indirect tensile asphalt cracking test). This last one has been recently accredited by ASTM and is one of the innovative ways to assess cracking resistance under indirect tension. It has proven to be very practical; it is easy to prepare since no cutting, notching, drilling, gluing, or instrumentation is needed [1], can be completed in 1 min and is considered repeatable [3], and needs only low-priced equipment. This test meets quality control requirements and succeeds in defining a unique index capable of sorting mixes' cracking resistance. Much of the literature described the test's sensitivity to the mix's components and to the test's conditions. This paper will focus on conducting the IDEAL-CT test while varying five main factors: air void content, loading rate, aggregate shape between high and low angularity, contact bond for two different aggregate types (granite and hard limestone), and two different mix gradations, including Superpave gradation and coarse high matrix binder mix (CMHB).

The IDEAL-CT, as described in ASTM D8225–19 [1], is a traditional indirect tensile strength test run at room temperature (±1 °C) with a cylindrical specimen with a 150 mm diameter at a loading rate of 50 mm/min with a thickness of 62 mm and a 7% air void content. Under this loading, a few cracks appear at peak-load and post-peak load up until failure. After two-thirds of the load have been dissipated in the post-peak curve, cracks propagate quickly and become increasingly more visible [3]. The post-peak point PPP75 (where the load is reduced to 75%) is used and measured from the load-displacement curve to calculate the cracking tolerance "CT index." The higher the CT index is, the better the cracking resistance in the field will be [1]. A detailed description of how this factor is calculated will be presented later in this report.

In light of the simulation technology revolution, the IDEAL-CT could be emulated in a computer model, reducing the cost and time needed to prepare and conduct lab tests [1]. While the finite element method (FEM) has been used in the past to model similar loading procedures, the choice

of using the distinct element method or discrete element method (DEM) relies on its popularity among fracture mechanics studies, its effectiveness in considering the particle shapes and model, and in its consideration of each element as an independent quantity. Also, a coupling of the FEM and the DEM method will be a better choice to cover unfractured areas on any model [6]; the DEM method has proven to be efficient for a sensitivity analysis [3], and thus it is used in this report. The Particle Flow Code in 2D is used to replicate the actual laboratory test. The software allows for the input of different shapes of aggregates, asphalt, and air voids by importing geometries and assigning each particle its own property. After that, the loading procedure is represented through a generation of a wall body moving downward, launching the free movement of the particles inside a cylinder shape acting as a boundary. Also, the algorithms generated described the interaction on a micro-basis between the particles considering the micro-shape of the mix, volumetric properties of the individual particles, and the interface's characteristics between components. It is based on a small increment of time, assuming that during a single time interval step, disturbance cannot cause a crack to propagate further from any particle than its immediate neighbor. Velocity and acceleration for each particle are constant during a single time step; a recurrent solution of Newton's second law of motion and the equations of force-displacement give a set of coordinates for each element at a given time, and the displacement versus load force curve can be depicted for each mix. Thus, the CT index can be determined after regressing the models' given curve.

2. Literature Review

The resistance of any given mix against cracking has been the focus of much research throughout the years. However, in the past few years, the focus has shifted to introducing new materials to the mix for the purpose of recycling previously used asphalt and including it into the mix. In this vein, the goal has been to improve cracking resistance, which requires monitoring the cracking performance of the asphalt samples.

Zhou et al. [3] have developed a sensitivity analysis for the IDEAL-CT based on the ASTM-D-8225–19 requirements. The test was compared to the Direct Compression Test (DCT), the Semi-Circular Bending test (SCB), the Indirect Tensile Test (IDT), the Overlay Test (OT), and the Bending Beam Fatigue test (BBF). It has shown an advantage over the others due to its practicality, repeatability, low coefficient of variation (COV), low-cost equipment, and more importantly, its sensitivity to the mix's components. The authors started by conducting multiple IDEAL-CT tests and computing the CT index for each different mix. The paper highlighted the results from mixes having different reclaimed asphalt pavement and shingles (RAP and RAS, respectively) components with a virgin mix; the virgin mix has the higher index, and different mixes with different binder types and different binder content show different results in their CT index. The best performance mix is the one with PG64–34 binder, and the higher the binder content is, the better the cracking resistance is. Also, the authors repeated the test on differently aged mixes and proved that the longer the mix is aged in the oven, the poorer the cracking performance will be. These tests show the sensitivity of the IDEAL-CT and its correlation with field performance.

Furthermore, Zhou et al. [3] conducted a repeatability statistical study for each previously mentioned mix, and a coefficient of variance less than 24% was obtained for every sample in question. Also, in a later study, Zhou et al. [10] developed a performance-related framework for quality control production in IDEAL tests emphasizing the comparison between the IDEAL-CT and the aforementioned tensile tests which showed a COV coefficient less than any of the other tests.

Many researchers used the finite element method (FEM) to model the IDEAL-CT. Some researchers found advantages in the use of the Lagrangian model base of the DEM over the Eulerian or the FEM method; their choice was based on the fact that the DEM emulates the reality well by describing a discontinuous space where the material can have different characteristics, while the FEM is based on the assumption of a continuous space. Even though the FEM method is computationally cheaper than the DEM, the latter gives a thorough study on the particle level. While other authors such as Monteiro [6] have presented the advantage of the DEM in modelling fracture mechanics; the higher the discretization is, the better the modeling procedure will be. A hybrid approach is introduced to describe the fracture mechanics of the mix coupling the DEM and FEM in order to apply the same study on larger areas; the DEM is used in the fractured zone, and the FEM in the surrounding areas.

Asphalt is a highly viscous material; still, many researchers relied on its elastic properties for modelling purposes. Saadeh et al. [2] described the contact between particles as elastic, defining their tensile and shear strengths as the point where the contact between particles exceeds this limit and the specimen breaks. On the other hand, Abbas et al. [7] divided the contact properties into two types; the contact between aggregates described an aggregate-aggregate contact model as linear elastic, and the mastic-aggregate behavior as viscous through the "burger" built-in model in the software used. The linear contact model is described using the normal and shear stiffness parameters, whereas the burger model is described using mechanical constants: shear and tension for viscosity. The burger model built-in contact property in the PFC2D software simulates the creep mechanism through the kelvin model acting in series with the Maxwell model: linear spring and dashpot components that act in parallel in one hand, with a combination of linear spring and dashpot components acting in series in the other. Moreover, in 3D analysis using the DEM on three different samples containing different types and percentages of asphalt binder, Han-Cheng et al. [4] used the linear elastic contact model, and a maximum deviation value of 2.88% between laboratory and model results was obtained.

In order to model the aggregate shape, X-ray or AIMS imaging techniques have been used to capture the aggregate materials. These techniques have been adapted to model ample tests where the shape of the aggregates is considered as a variable. For instance, Kim et al. [8] used high resolution imaging techniques to model the disk-shaped compact tension test. Han-Cheng et al. [8] scanned the aggregate using a high-accuracy camera to obtain a series of digital images, and the profile boundary of the aggregates was then reconstituted through programming. Abbas et al. [7] used an image analysis technique to capture Hot Mix Asphalt (HMA) microstructure. Grayscale images were processed into black and white images measuring 250 pixels wide by 400 pixels high, and each pixel represents not only the binder but also a portion of the aggregate fines. Saadeh et al. [2] performed the SCB test's numerical evaluation using the DEM, in which images of the aggregates were taken using the aggregate image measurement technique (AIMS), and the images were imported into the Particle Flow Code in Two Dimensions software (PFC2D) as geometries in order to consider the angularity and dimension of each aggregate.

The angularity and exact dimensions of the aggregates directly impact the contact surface between aggregates. Furthermore, Mahmoud et al. [12] concluded that the mixes with high angularity have a higher peak load before failure than the mixes with a low angularity index, for coarse matrix high binder (CMHB) mixes with a semi-circular bending test (SCB), while it is the other way around for the Superpave mixes. Higher aggregate angularity allows better interlocking and yields to a uniform distribution of contact forces in the case of the CMHB. Abbas et al. [7] performed an analysis comparison with the Standard Penetration Test (SPT) results on different HMA percentage mixes where aggregate angularity and particle size distribution were controlled in the analysis through the use of multisided polygons of different size, concluding that an increase in the aggregate's angularity leads to an increase in the mix's strength.

The specimen used in the IDEAL-CT test's numerical model is a mix of mastic aggregates and voids. The mastic itself is a combination of asphalt binder and aggregate material passing sieve No. 8 (2.36 mm). Effectively, Saadeh et al. [2] and Mahmoud et al. [12] stated that modelling aggregates smaller than sieve No. 8 cause major delays in the simulation and produce unexpected results, so aggregates passing sieve No. 16 (1.18 mm) were ignored. Furthermore, Han-Cheng et al. [4] performed a numerical analysis on a 3D model using a PFC3D model analysis with particle sizes ranging from 0.075 to 19 mm, and other fine particles were added to the mastic portion. Saadeh et al. [2] performed a calculation based on the volumetric properties of the mix and its gradation size, and while importing the geometries in the model, a generation of clumps was rendered. Each clump size was based on the sieve size opening of the sieve analysis, and the number of clumps was deducted from the volumetric percentage of each component combined with sieve gradation analysis. Air voids were modeled as well in clump bodies with a 1 mm diameter, and the mastic filled the remaining areas. The representation of aggregates as clumps with specific properties was also adapted by Abbas et al. [7] in order to emulate a more realistic model.

Zhou et al. [3] experimentally proved that the binder type and content influences the CT index and, as a result, affects cracking performance on the road. The "PG64–34" has demonstrated the best cracking resistance performance, and the test was demonstrated to be sensitive to the binder percentage. Also, in his 3D modeling, Han-Cheng et al. [4] performed a comparative study and found that after adding carbon nanofiber with different percentages in the asphalt mix, fractures were distributed abundantly in the mix with the most carbon fiber added. While Mahmoud et al. [12] studied the strain energy release rate of nine different asphalt mixtures, the asphalt mixtures contained four types of asphalt binders and two nominal aggregate sizes, and the results showed the impact of the binder content and type on the mix's performance.

Additionally, a study by Kim et al. [9] proved that angularity has a direct impact on resistance to fatigue damage. The study was conducted both in the laboratory and in a finite element micro-modelling of the static creep test and the asphalt pavement analyzer test (APA), proving that while high angularity aggregates are more desired, they showed a decrease in crack resistance due to the concentration of the stresses and forces on the sharp edges of high angularity aggregates.

Moreover, Zhou et al. [3] proved that the IDEAL-CT is sensitive to air void content using the Plackett-Burman (PB) matrix and that the air void variable is the most impactful parameter of all three variables affecting the IDEAL-CT used in the study, which included specimen thickness and temperature. Meanwhile, Abbas et al. [11] focused on air void distribution, size, and orientation by conducting a uniaxial static creep 3D-model test and demonstrated from the simulation results that the increase in air void content resulted in greater creep strain. Previously, most of the modelling techniques illustrated the air voids as objects with no mass. Mahmoud et al. [12] introduced air voids in the model as circular clumps with a 1 mm diameter after aggregate

generation based on their volumetric percentage, and air voids were not assigned any density. After contact bonds are created and particles' properties are generated, these clumps were deleted to imitate the real mix.

3. Objective

The objective of this study is to find an economical substitution for the expensive laboratory tests needed to study the sensitivity analysis of the indirect tensile test using a software that is proven able, with correct calibration, to yield a result that is comparable to that of an actual test.

4. Methodology

The IDEAL-CT test modelling analysis using the DEM method was achieved through PFC2D software (Particle Flow Code two-dimensional program). The modelling procedure allows a rigid assembly of various-sized particles to move through translation and rotation, and bodies can interact based on internal forces and moments dictated by the contact model, which is specifically adapted for each type of material being simulated. Generally, three types of model components can be generated: clumps, balls, and walls in 2D models. Wall motion does not obey the equations of motions. Geometries and model components are created and generated in a domain. The domain in PFC2D software represents a geometric space where the model components can exist. The size and location of the domain is user-defined, and the condition of the domain is chosen by the user to determine what will happen to objects falling outside the domain. Generally, the user has four options regarding bodies outside the domain: (1) the stop condition where the velocity and the spin of the objects are nulled outside the domain; (2) the reflect condition where bodies that move outside the simulation domain are reflected back into the domain with their velocity reversed, such that if a body falls outside the domain, it is sent back in the opposite direction; (3) the periodic condition where the bodies falling outside the domain are brought back inside, and finally (4) the destroy condition which deletes balls and clumps and even wall facets that move outside the domain. The destroy condition is applied for the modelling in this project because it matches the state of testing where the specimen fails or is destroyed after the test is complete.

After defining the model domain, model bodies can be generated inside the box domain defined as a 165 x 150 mm rectangular box. Aggregates and mastic can be modeled using balls as rigid disks with an assigned mass, unit thickness, and radius. However, using this method, the shape of the aggregates cannot be considered, and thus neither can the interlocking, texture, or angularity of the aggregates be used. Clumps, on the other hand, are an assembly of circular pebbles that can also rotate and translate and act as a single ball. The shape of these particles can be controlled through several methods. In this project, clump templates are created through the generation of AutoCAD shapes imported as geometries in the software. This procedure will be explained further in the following section. Clump motion obeys Newton's second law of motion. The interaction of clumps can also be measured through internal contact forces and moments. While balls and clumps can illustrate the aggregate or object phases, walls—represented as lines in 2D—can be introduced as a barrier or loading condition in the model. These segments do not comply to the equation of motion but can translate and rotate, and their velocity can be assigned through the attribute command. The bodies are described in the figure below.

Figure 1. PFC Model Bodies and Contacts

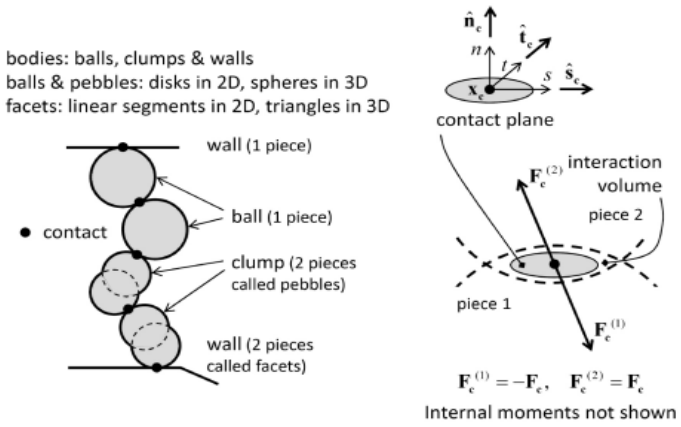

The modelling procedure in PFC2D software gives the user the advantage of controlling surface areas and introducing complex geometries into the model, modelling the exact shapes of aggregates through an advanced imaging technique. Aggregates are placed on a circular platform under light and cameras, and a high-resolution image is taken for the aggregates in question. Then, the aggregates are divided with respect to their angularity index, and these images are imported into the program as geometries and assigned a certain distribution and mass properties.

Another crucial step in modelling the IDEAL-CT is to determine the type of contacts between the components of the models: contact between aggregates, contact between mastic particles, and aggregate-mastic contact. The program has two general options to define contact behaviors between objects: through a complex mechanical behavior using fish functions or through the embedded contact models or contact model assignment table (CMAT).

The methodology is described only briefly above and will be articulated in more detail in the following section, which describes the work done to model each mix in each scenario. Following the work conducted by Saadeh et al. [2], the sensitivity analysis in this report was done based on the Plackett-Burman sensitivity analysis (PBSA) methodology. In general, the Plackett-Burman (PB) matrix is used to reduce the number of scenarios when more than four variables are being considered for an individual mix. In this study, the sensitivity analysis is conducted for two factors, air void content and loading rate, for every type of mix. PBSA was implemented to test two varying parameters at the same time, clearly illustrating which factor would be most impactful.

Applying the PB matrix for two variables can be done by choosing an upper and lower value (using a small increment) for each of the particles: varying the air voids by 1% ($7\% \pm 1\%$) and the loading rate by 0.025 m/s (0.05 ± 0.025), as shown in the table below for each different mix. The same sensitivity study was conducted for two different mix types: CMHB gradation granite and hard limestone samples.

Table 1. PB Matrix for Sensitivity Analysis

Scenarios	Air Void Content (%)	Loading Rate (m/s)
1	6	0.0475
2	6	0.0525
3	8	0.0475
4	8	0.0525

The number of each scenario above will be used to refer to the air void percentage and loading rate used in the following report. The following steps, presented as subsections, were done in order to recreate the IDEAL-CT model.

4.1 Aggregate Shape Analysis

The first step of the modelling process is to import the aggregates into the software. Many studies previously modeled the aggregates as circular particles or balls. In a sensitivity study, considering aggregates as balls in the simulation could yield a successful sensitivity answer. However, aggregate shape influences the cracking resistance of the mix; it is known that flat and elongated particles tend to break under traffic. Hence, aggregate shape is crucial when studying premature pavement failures. For cracking resistance studies, the SCB test conducted by Mahmoud et al. [12] proved that the angularity of aggregates influenced the peak load prior to breaking for the mix, positively for mixes where the aggregates are the majority and negatively when the mastic particles dominate the cylinder's volume. Therefore, interest in introducing the aggregate shape as a variable has risen again. Since the aggregate angularity was considered as a variable in the comparison procedure, the angularity index of the aggregates was taken into consideration. The angularity analysis conducted in the studies of Saadeh et al. [2] and Mahmoud et al. [12] was utilized in this study.

The angularity index is a measure that describes the particle's contour, determining whether it is rounded or angular. Abbas et al. [7] considered an index less than 2100 as a low angularity index particle and an index higher than 2100 as a high angularity index particle. Based on this approach, the classification of particles based on their angularity was accomplished by Mahmoud et al. in the following graphs. A total of 135 low angularity aggregates are presented below in Table 2, and their angularity index values are represented in Figure 2 below. Additionally, 155 high angularity aggregates are presented below as images in Table 3 and classified as per their index in Figure 3. These images were taken from Mahmoud et al. [12] for SCB test modelling.

Figure 2. Angularity Index for Low Angularity Aggregates

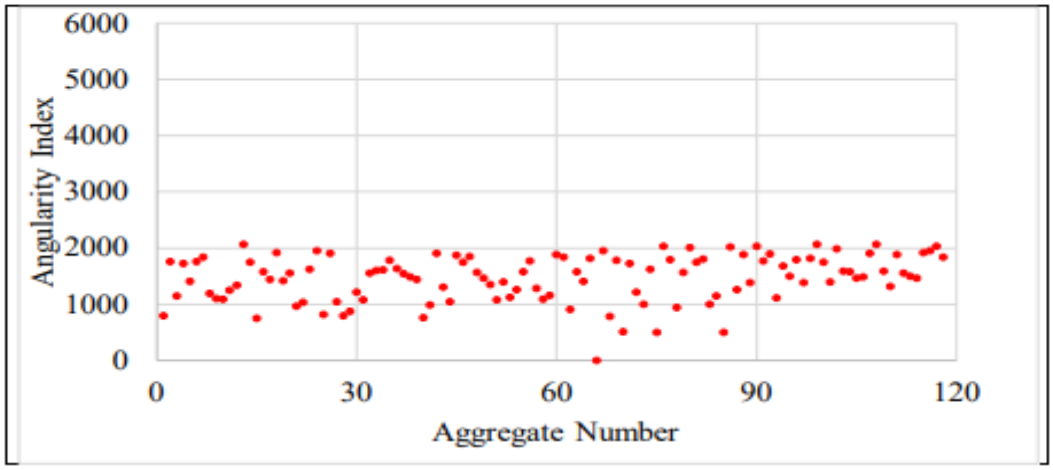

Table 2. Low Angularity Aggregates

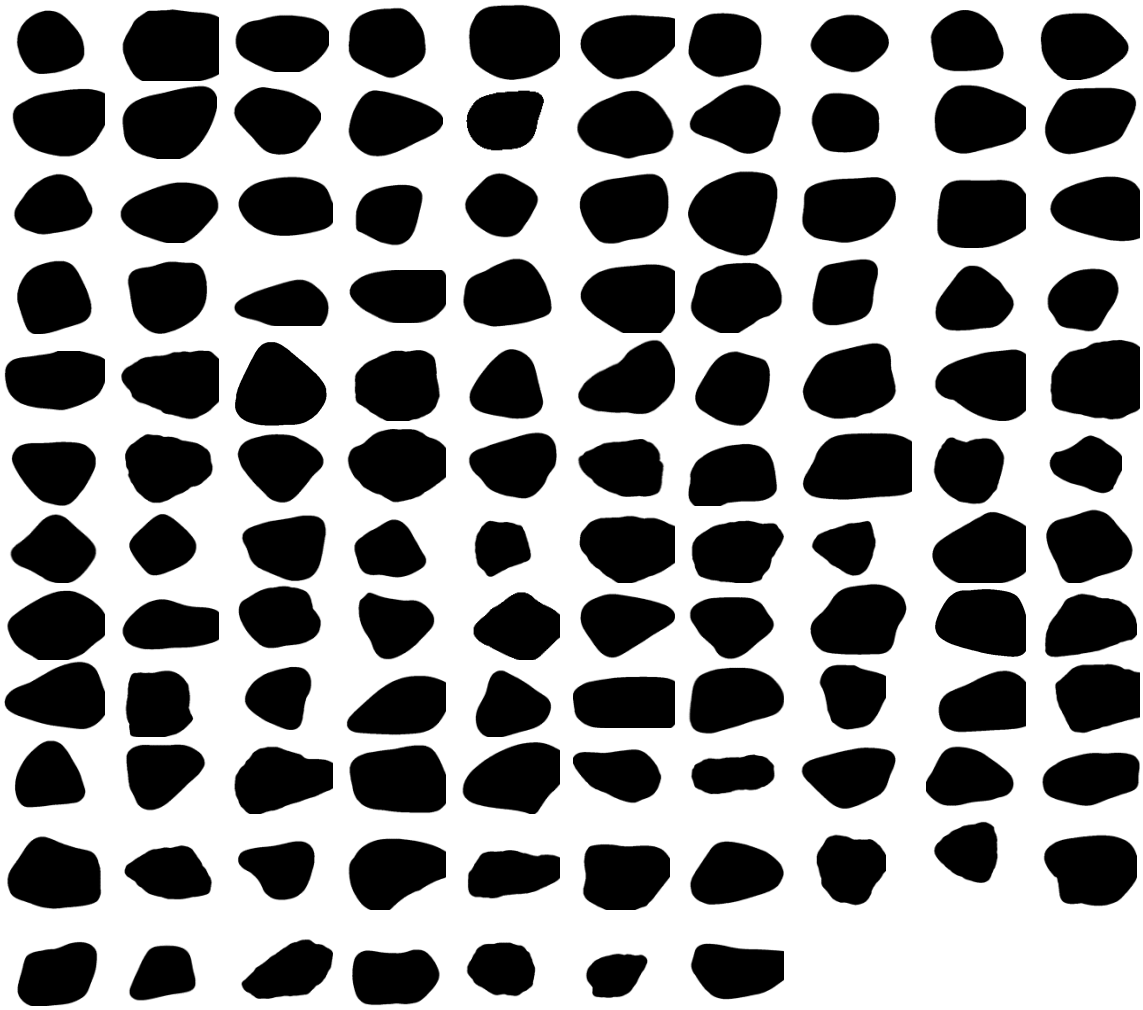

Figure 3. Angularity Index for High Angularity Aggregates

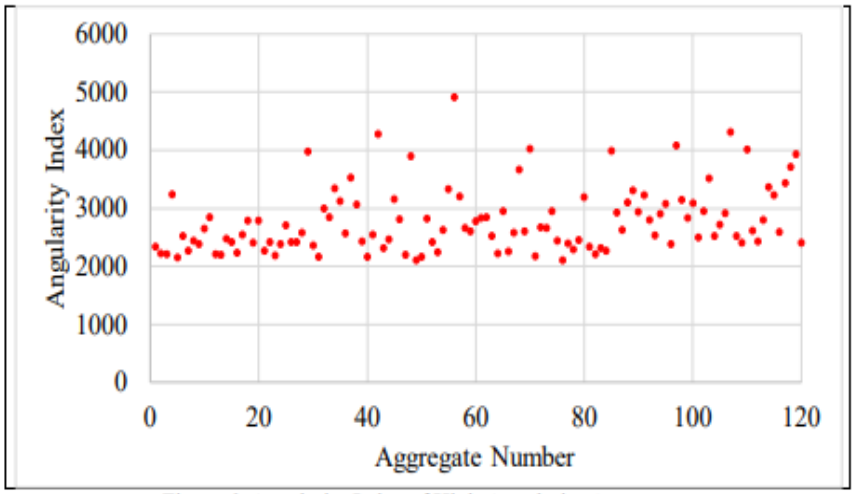

Table 3. High Angularity Aggregates

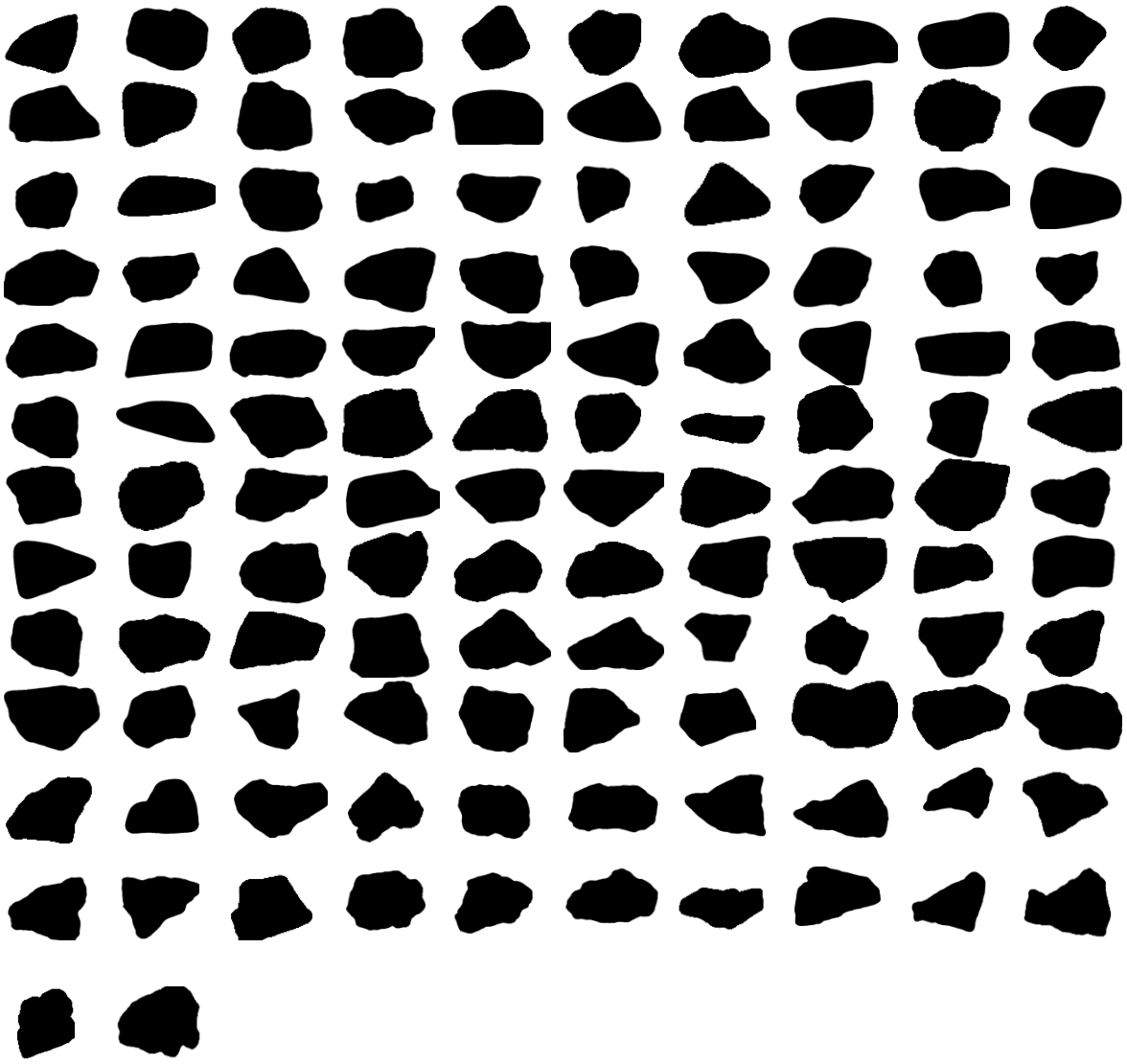

The aggregate shape was captured using the aggregate image measurement system (AIMS), as seen in Figure 4 below and then was imported into AutoCAD software. Contour lines were drawn around each aggregate's shape and files were imported as geometries in the PFC2D software.

Figure 4. AIMS Procedure

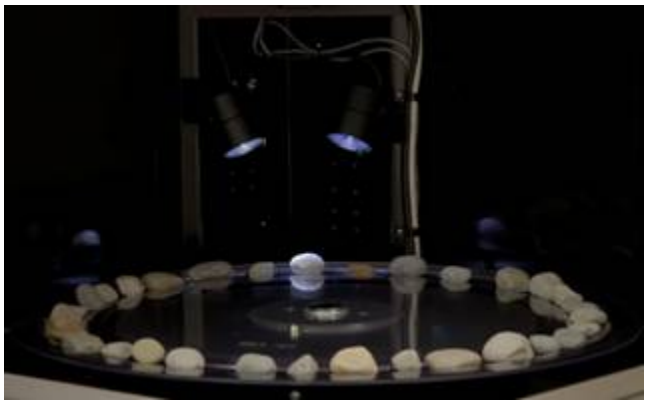

The geometry commands in the software allow the user to import any shape needed during the modelling procedure, to create a shape, and even to export a shape from the model. These geometries can later be used to create any type of particle, but by themselves geometries are not considered model components and hence can be created anywhere in the model.

These geometries are then used to create clump templates representing a total of 290 different aggregate shapes and sizes, and then should be placed inside a model domain, otherwise the specified domain condition will be applied for bodies falling outside the domain.

4.2 The Volumetric Relationship of Different Aggregate Mixes

As extensively described in the literature review before, the cracking resistance of a mix depends on the quantity of asphalt and aggregate and the type of bond they share. For this reason, two general mixes were used: Superpave gyratory mix and a coarse high matrix binder mix (CMHB). A correct modelling technique would be able to emulate the quantity of aggregates versus asphalt. It would also be able to represent aggregates as per their correct size, thus aggregates were modelled based on the gradation size obtained from the sieve analysis conducted by Alvarado et al. [5] and their volumetric properties.

Volumetric relationships correspond to the area (volume in 3D analysis) filled by each of the mix's components. The volumetric properties are taken from Alvarado et al. [5] and then updated for every mix in order to conduct the sensitivity analysis. Mixes used in previous studies had a 4% air void using the phase diagram in Figure 5 below, and based on the following formulas, the percentage of each component was calculated for every different air void percentage used.

Figure 5. Volumetric Phase Diagram

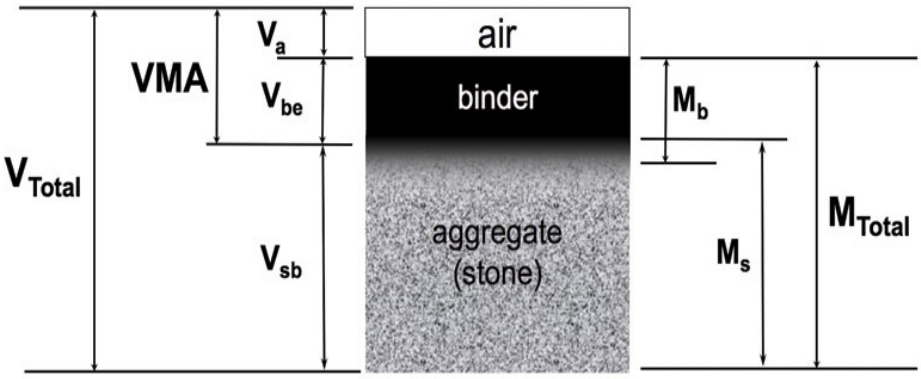

The theoretical maximum specific gravity, the bulk specific gravity of aggregates, and the binder content of every mix was taken from Alvarado et al. [5], and then the following steps were done to complete the volumetric study:

1. Calculate the effective specific gravity of aggregates:

$$G_{se} = \frac{100 - P_B}{\frac{100}{G_{mm}} - \frac{P_b}{G_b}} \quad (1)$$

   Where the binder specific gravity is considered to be 1.2.

2. Calculate the bulk specific gravity of the mix using the air void content of each mix and the theoretical maximum specific gravity.

$$AV = \left(1 - \frac{G_{mb}}{G_{mm}}\right) 100 \quad (2)$$

3. Assume the total volume of the mix equals 100 m^3 and calculate the total weight as follows:

$$W_t = G_{mb} \times V_t \quad (3)$$

4. Calculate the binder weight and volume using the binder content percentage and the total weight. Then, calculate the volume using the weight divided by 1.2, which is the asphalt's specific gravity.

$$W_b = W_t \times P_b \quad (4)$$

$$V_b = W_b / 1.2 \quad (5)$$

5. Calculate the aggregate weight, and since the air void has no mass, the weight of the aggregates will be the difference between the total weight and the asphalt's weight.

6. Calculate the effective specific volume of the aggregate and the bulk specific volume of the aggregate using the aggregate's weight and density.

To summarize the calculation procedure described above, the analysis took into account two different gradations. Additionally, two different materials were considered for the analysis: hard limestone and granite. Each material has a different gradation and different volumetric properties. The following tables are a representation of the calculation described above for the 7% air voids for the four mixes in question.

Table 4. Volumetric Relationship Calculation for 7% Air Voids

Property	Hard Limestone		Granite	
	CMHB	Superpave	CMHB	Superpave
Binder content	4.20	4.00	5.30	4.80
Sieve size (in)	Percent passing (%)			
1	100.00	100.00	100.00	100.00
0.75 (3/4)	99.00	99.00	99.00	99.00
0.492 (1/2)	78.50	95.00	78.50	95.00
0.375 (3/8)	60.00	92.50	60.00	92.50
0.187 (No. 4)	37.50	77.50	37.50	77.50
0.0929 (No. 8)	22.00	43.00	22.00	43.00
0.0469 (No.16)	16.00	30.00	16.00	30.00
0.0029 (No. 200)	7.00	6.00	7.00	6.00
G_{mm}	2.55	2.57	2.47	2.52
G_{sb}	2.70	2.72	2.60	2.66
G_{se}	2.69	2.70	2.63	2.67
Air voids	7.00	7.00	7.00	7.00
V_t	100.00	100.00	100.00	100.00
G_{mb}	2.38	2.39	2.30	2.34
W_t	237.52	239.20	229.80	234.36
W_b	9.98	9.57	12.18	11.25
W_s	227.55	229.63	217.62	223.11
V_{sb}	84.40	84.58	83.67	84.03
V_{se}	84.69	85.03	82.85	83.63
V_{be}	8.60	8.42	9.33	8.97
V_b	8.31	7.97	10.15	9.37
Fine Aggregates	23.00	36.00	22.00	43.00
Percent Fine	19.48	30.61	18.23	35.96
Coarse Aggregate	65.21	54.42	64.62	47.67
Mastic	27.79	38.58	28.38	45.33

The sensitivity analysis conducted in this report focuses on the change in air void percentage. Therefore, each mix has been simulated for a 6% air void content (Scenarios 1 and 2) as well as 8% air void content (Scenario 3 and 4). The 7% air void is used for comparison between the other two mixes. The two different air void contents were used to demonstrate the sensitivity analysis of the IDEAL-CT towards a small change in air void such as 1%, as per the Plackett-Burman method described above. The following table will summarize the volumetric relationship calculation for every different air void percentage.

Table 5. Component Percentage Summary

Property	Hard Limestone		Granite	
	CMHB	Superpave	CMHB	Superpave
7% Air Void				
Coarse Aggregate	65.21	54.42	64.62	47.67
Mastic	27.79	38.58	28.38	45.33
6% Air Void				
Coarse Aggregate	65.91	55.00	65.32	48.18
Mastic	28.09	39.00	28.68	45.82
8% Air Void				
Coarse Aggregate	70.37	58.88	63.93	47.15
Mastic	21.63	33.12	28.07	44.85

4.3 Sieve Gradation Analysis

The sieve gradation analysis is important in determining the size of the aggregate phase in order to create an accurate model. Sieve gradation was conducted by Alvarado et al. [5], where sieves are placed on top of each other starting with the coarsest sieve at the top and increasing in fineness the lower each sieve is placed. After that, Table 6 shows the percentage of the total weight of the aggregate retained before passing to the next sieve. In the modelling procedure, coarse aggregates retained up to sieve Number 8 are the only aggregates considered; smaller particles have proven to cause unnecessary delays and yield inaccurate results as per Alvarado et al. [5], Saadeh et al. [2], Mahmoud et al. [12], and various simulation research. Aggregates passing sieve Number 8 were added to the mastic phase (pointed out as %fine in Table 4), and the updated gradation sieve analysis is represented in Table 7 below (Tables from Mahmoud et al. [12]).

Table 6. Gradation Analysis for Different Samples

Sieve #	Sieve Size (mm)	% Retained	
		Coarse Matrix High Binder	Superpave
1”	25.4	0	0
0.75”	19.05	1	1
0.5”	12.7	21	4
0.375”	9.53	19	3
4	4.75	23	15
8	2.36	16	35
16	1.19	6	13

Table 7. Updated Gradation Analysis for Different Samples

Sieve #	Sieve Size (mm)	% Retained		Area of the Opening (mm^2)
		Coarse Matrix High Binder	Superpave	
1”	25.4	0	0	506.71
0.75”	19.05	1	2	285.02
0.5”	12.7	26	7	126.68
0.375”	9.53	24	4	71.26
4	4.75	29	26	17.72
8	2.36	20	61	4.37
16	1.19	0	0	-

The area of each sieve opening will be used as the size of each aggregate retained by that sieve. In PFC2D, the user can control their area, so after importing the geometries presented in Tables 2 and 3 for high or low angularity index aggregate models, they can compute the volumetric and size properties for the aggregates. Clump templates can be created as geometries with circular balls inside in the shape presented in 4.1 Aggregate Shape Analysis and the size regulated as per the tables above.

4.4 Particle Generation

The modelling procedure started by first drawing the outline of the aggregates in AutoCAD, imported in the model software as described in the first paragraph of the methodology. These geometries were used to create clump templates representing the aggregate phase. The user can assign their area, which is assumed to be equal to the sieve opening size and the number of the aggregates based on Table 7. The generation of the aggregates was accomplished randomly inside a circular disk of 150 mm diameter inside a rectangular domain.

In order to evaluate the repeatability of the IDEAL test through different aggregate generations, approximately 20 to 25 different mixes were generated for each mix case, varying only the distribution of the particles inside. The following sketches show the procedure for the creation of aggregate clumps for both CMHB and Superpave mixtures. Only a few sketches out of the 20 to 25 different generations are represented below. The clumps are divided by size, and the number assigned to each group corresponds to the diameter opening in mm for each corresponding sieve. The generation procedure started with the sieve with the largest opening to the sieve with the smallest, as shown below.

Figure 6. Clump Aggregate Generation for CMHB Mixture Samples

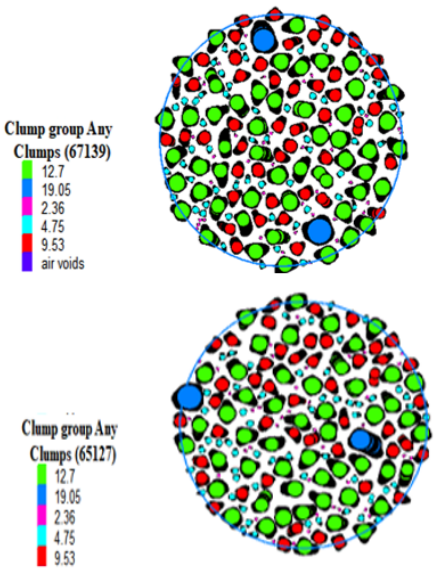

Figure 7. Clump Aggregate Generation for Superpave Mixture Samples

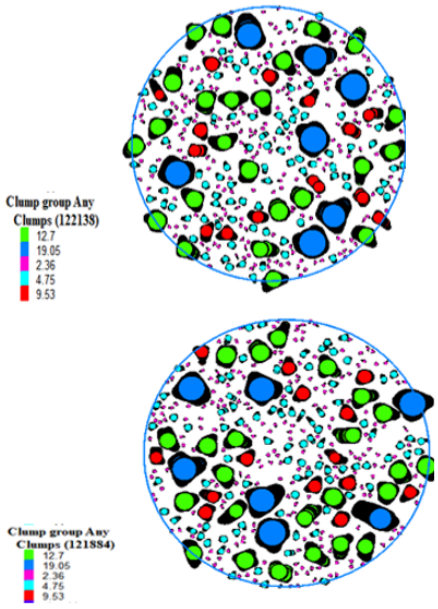

After aggregate generation, air voids are added as per their percentage in each gradation (6%, 7%, or 8%). Air voids were modelled as circular clumps with diameters of 1 mm generated from the model in accordance with Mohamad et al. [12]. Also, the generation of air voids is random through the modelling procedure, and their position changes from one sample to another just like in other aggregate clumps. The following figure represents the addition of air voids in the two different mixtures.

Figure 8. Aggregates and Air Void Generation in CMHB Mixture Samples

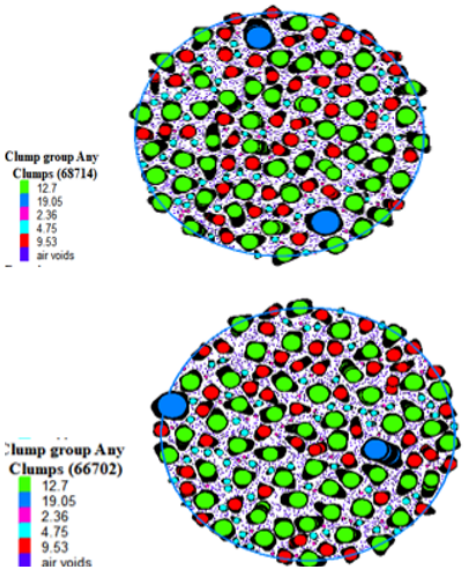

Figure 9. Aggregates and Air Void Generation in Superpave Mixture Samples

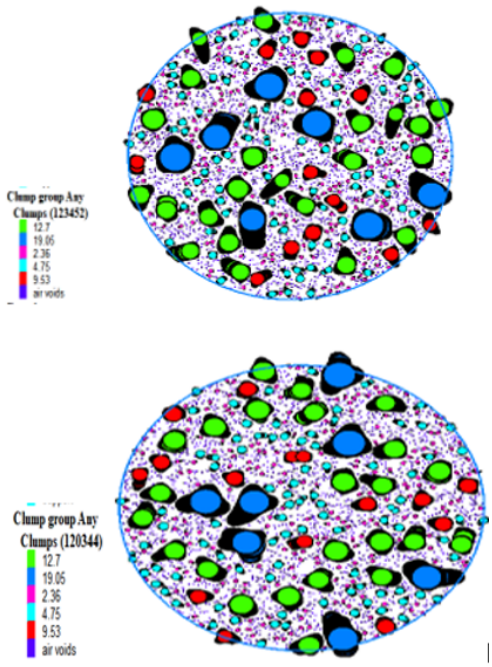

Once the first part of representing the particle is done, the main purpose is to model the IDEAL-CT shape, and the remaining area inside the 75 mm radius circle should be filled with asphalt particles. Boundary conditions are introduced as a rectangular domain.

The recreation of the IDEAL shape is simple; it's composed of a circular wall with a 75 mm radius filled with circular balls representing the asphalt, as shown in the figure below. The balls' diameters range from 0.2 mm to 0.6 mm in accordance with Mahmoud et al. [12] in their replication of the SCB test, where this packaging aims to create a dense packing system. In order to generate balls inside the model circle, the method adapted was to assign a target porosity of 0.1 with a damping ratio of 0.7 randomly. Then, the system was set to an equilibrium state with the purpose of dissipating the balls' energy, preventing any possible overlapping and simplifying further simulation. Then the model shape was saved.

After creating the dense assembly, every sample of the mix presented in the figures above is imported inside the IDEAL shape. The model shown in Figure 10 below represents the mix with all its components.

Figure 10. IDEAL Dense Packing Scheme

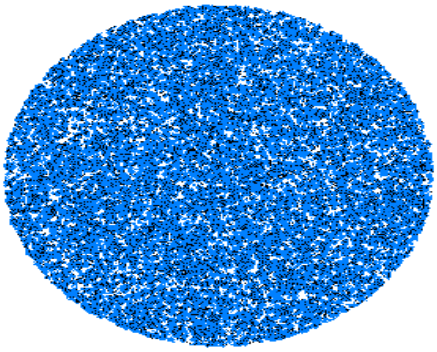

Figure 11. IDEAL Samples for Superpave Mixes

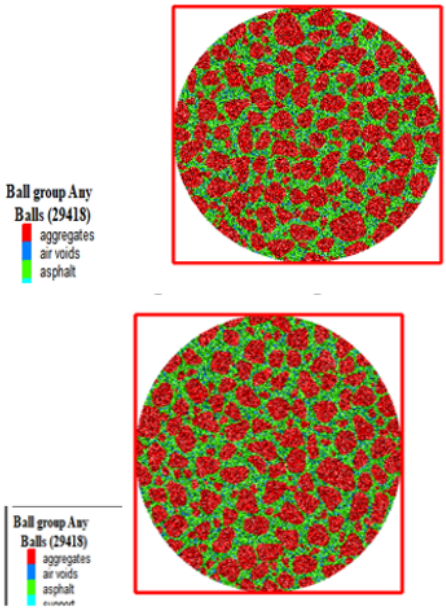

Figure 12. IDEAL Samples for CMHB Mixes

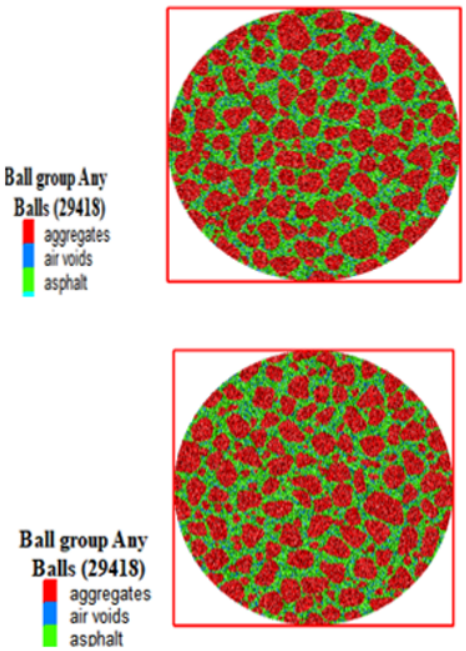

A total of 29,418 balls were generated for each sample in each mix, representing the three model components—air voids, aggregates, and asphalt—inside a circular wall with a 75 mm radius. Thereafter, the wall circumference can be deleted alongside the air void balls for a more accurate representation. The distribution of the particles inside a circular shape is presented in the figure below.

Figure 13. IDEAL Model for the Superpave Mixture

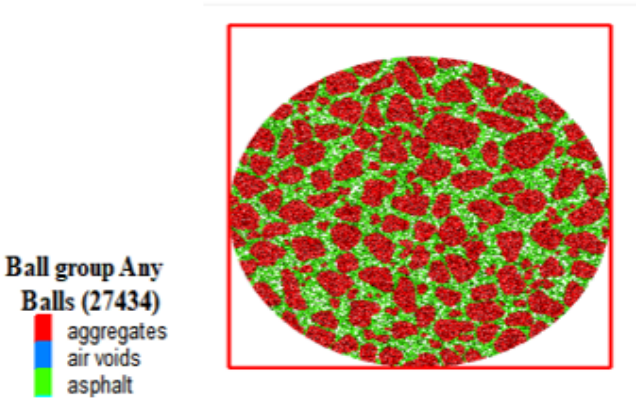

Figure 14. IDEAL Model for the CMHB Mixture

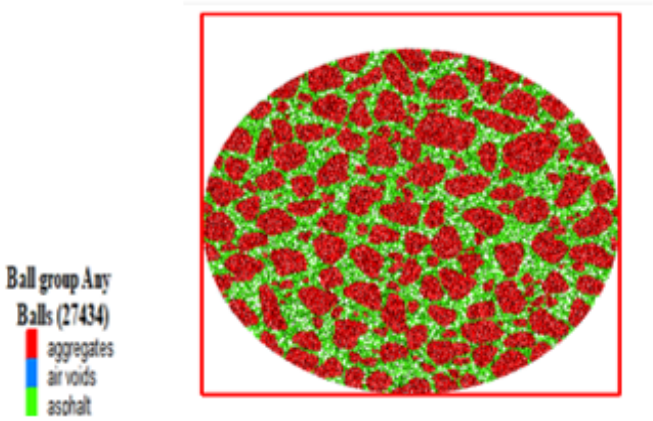

As mentioned before, the contact type adapted in this model, between aggregate particles, mastic bodies, and aggregate and mastic, is the linear contact bond model, which is an embedded model in the CMAT table and is already defined in the PFC2D software.

The linear contact bond, as shown in the figure below, represents a couple of elastic springs and inactive dashpots with both normal stiffness and shear stiffness with specified shear and tensile strengths. If the forces between any two particles exceed these defined strengths, the bond between the particles breaks. When this breakage occurs, the bond ceases to exert normal and shear forces, effectively setting them to zero. Contact bonds prevent any slip, and the shear force will be equal to the product of the friction and the normal force. This linear contact model is called "bonded" because no slip can occur. Otherwise, the model would be a linear elastic model. Figure 15 sketches the difference between the two cases.

The contact model is activated when the gap between particles becomes zero; at that point the force displacement law can be applied, and both linear and dashpot forces can become tensile. Whenever the forces exceed the limit set by the user, the bond breaks, as shown in the Figure 16.

Figure 15. The Linear Contact Bond Model vs. the Unbonded Model

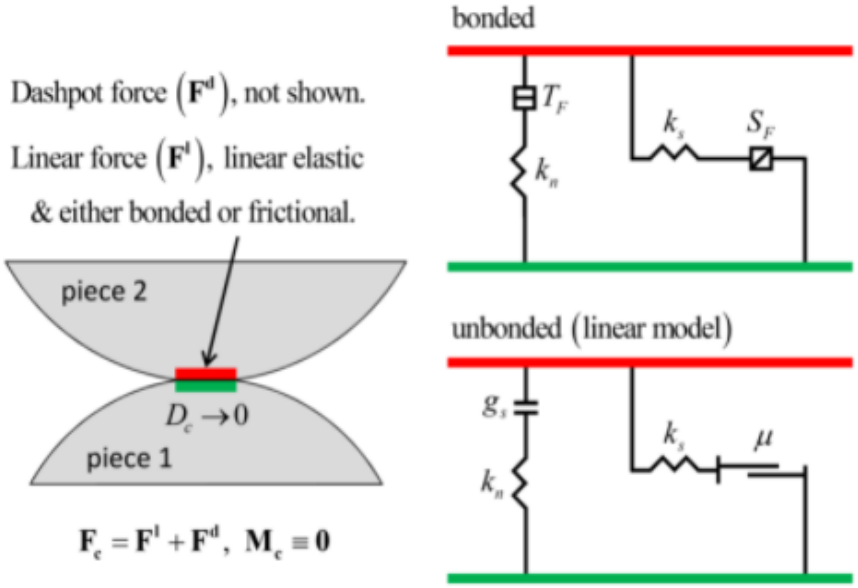

Figure 16. The Linear Contact Bond Model in Shear and Tensile Strengths

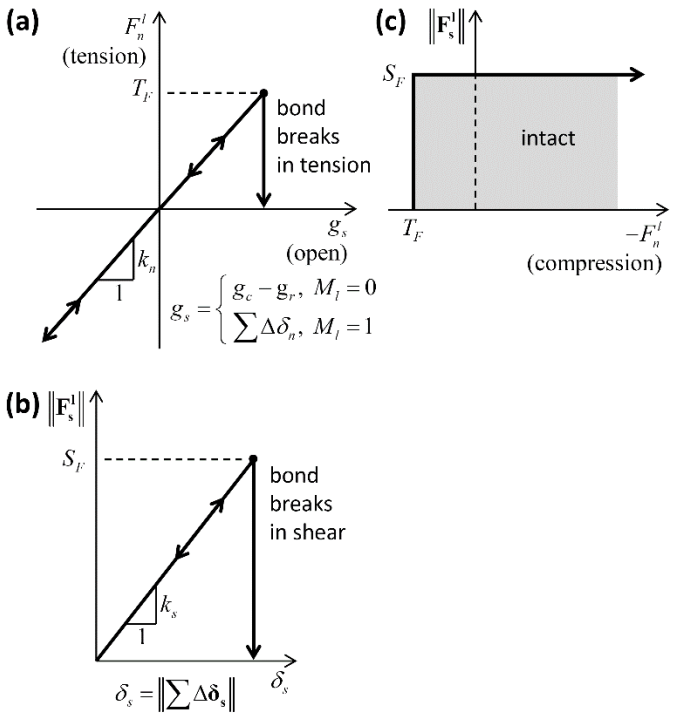

In order to define and establish the model, the user should be able to input the effective modulus of the particles, the normal to shear stiffness ratio, and the shear and tensile strengths of the particles, as shown in the figure below.

Figure 17. Linear Contact Bond Model Input Methods

Method	Arguments	Symbol	Type	Range	Default	Description
Linear Group:						
area						Set user_area to the area
deformability						Set deformability
	emod	E^*	FLT	$[0.0, +\infty)$	N/A	Effective modulus
	kratio	κ^*	FLT	$[0.0, +\infty)^*$	N/A	Normal-to-shear stiffness ratio
Contact-Bond Group:						
bond						Bond the contact if $g_c \in G$
	gap	G	VEC2	$\mathbb{R}^2$	$(-\infty, 0]$	Gap interval
unbond						Unbond the contact if $g_c \in G$
	gap	G	VEC2	$\mathbb{R}^2$	$(-\infty, 0]$	Gap interval
cb_strength						Set tensile and shear strength
	tensile	T_σ	FLT	$[0.0, +\infty)$	N/A	Tensile strength [stress]
	shear	S_σ	FLT	$[0.0, +\infty)$	N/A	Shear strength

Prior to assigning any contact models, the mastic and aggregates should be assigned a mass in accordance with the laboratory tests and modeling conducted by Alvarado et al. [7]. Since the same gradation and material are adapted, the density was assumed to be the same 2600 kg/m^3 for granite aggregate,1500 kg/m^3 for granite mastic, 2700 kg/m^3 for hard limestone aggregate, and 1500 kg/m^3 for hard limestone. Elasticity modulus and contact bond properties were taken from Mahmoud et al. [12]. Following the work done by Alvarado et al. [6], extensive calibration procedures, as published in these previous studies, are used in the sensitivity analysis. The following table summarizes the parameters used in this report.

Table 8. Particle Properties

	Granite		Hard Limestone	
Property	**Aggregate**	**Asphalt**	**Aggregate**	**Asphalt**
Elasticity Modulus (GPa)	1.5	0.03	2.3	0.023
Shear strength (GPa)	1.5	1.5	1.5	1.5
Tensile strength (KPa)	510	87.5	375	102.5

The calibration procedure conducted previously also relied on the PFC2D software and laboratory tests. After conducting laboratory tests, an X-ray image of the microstructure captured the specimen, and then a Fortran code was used to differentiate between mastic and aggregate particles.

Three tests were conducted to determine the particles' properties: a modulus test to determine young modulus of particles, a compression test to determine aggregate properties, and then an indirect tensile test to determine mastic properties. This general procedure is used to modify the contact stiffness so that the model results matched the experimental results.

In the modulus and compression tests, aggregate samples of 2 x 2 inches were tested using balls with a diameter of 14.2 mm and a density of 160 PCF, as shown in the figure below.

Figure 18. Model Used in the Compressive Strength Test

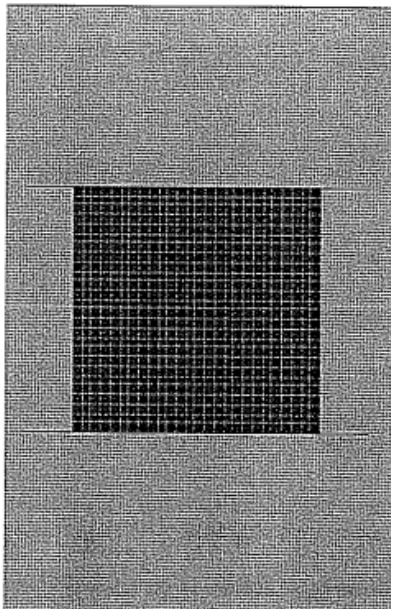

A loading rate of 1.2 in/s was selected for the compressive test. The normal and shear strengths were varied until the numerical results best matched the experimental results using a friction of 0.5 and a value of unity for the shear to stiffness ratio. The following graphs demonstrate the calibration results. The same procedure was used for both granite and hard limestone to determine aggregate characteristics. The same procedure was adapted by Mahmoud et al. [12] as well, and the same results were obtained and then used in Saadeh et al.'s [2] SCB modeling, as well as in this study. The curves presented below are the results obtained by Mahmoud et al [12].

Figure 19. Aggregate Calibration Test for Tensile Strength

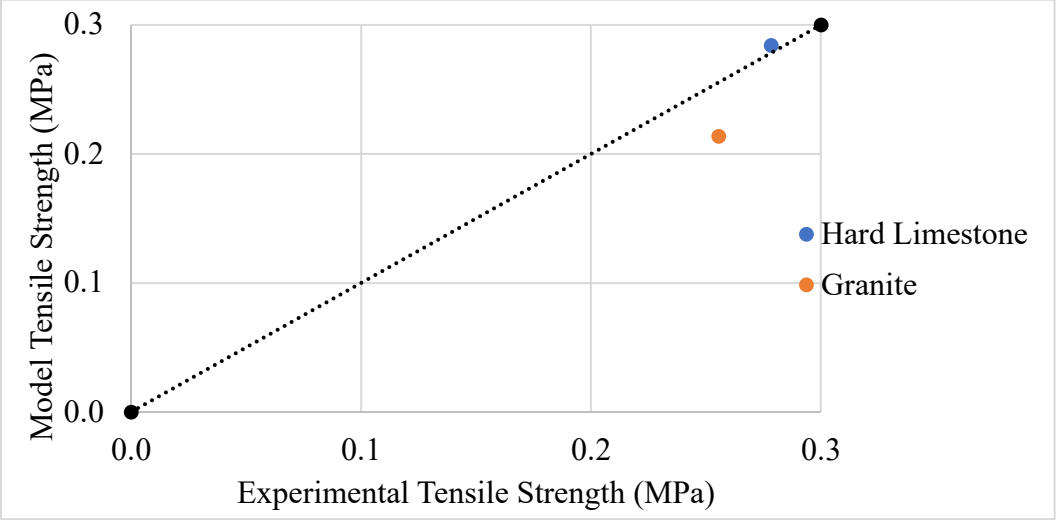

Figure 20. Aggregate Calibration Test for Compressive Strength

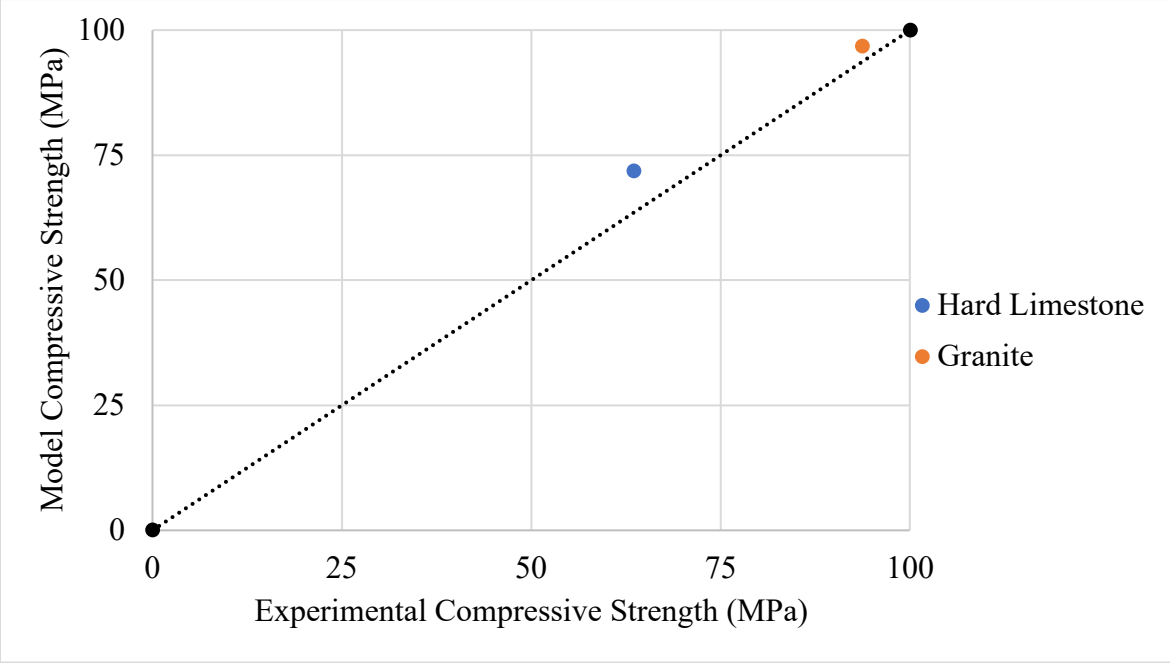

Figure 21. Aggregate Calibration Test for Elasticity Modulus

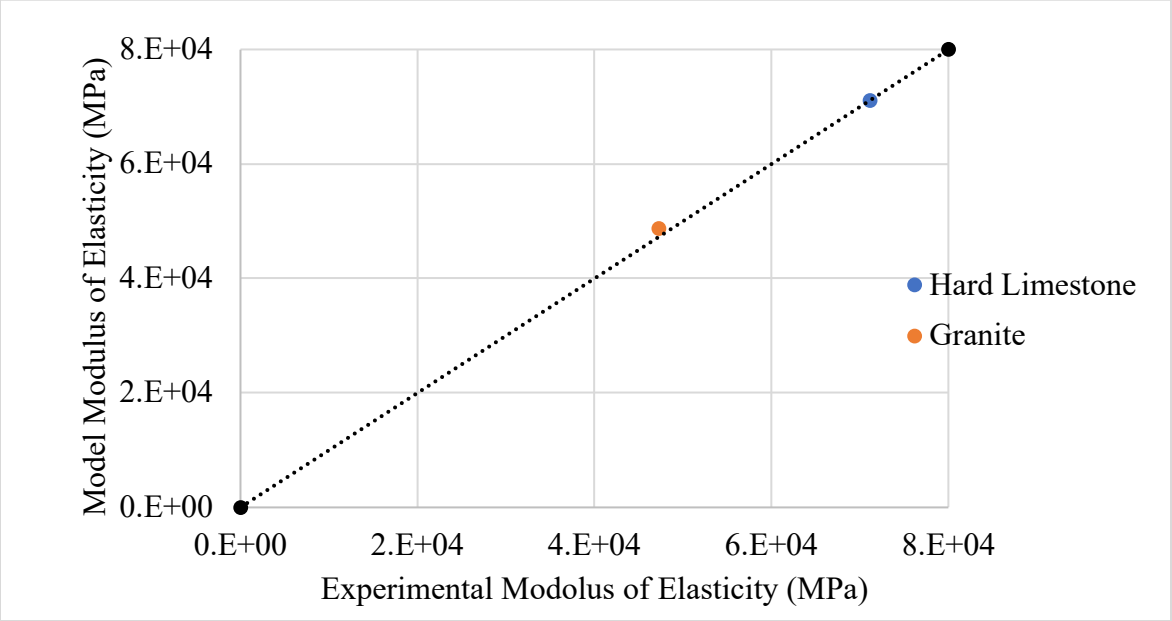

The results obtained from the aggregate calibration are used to model the indirect test of an HMA mix for both types of asphalt, mastic, granite, and hard limestone, using the model below created by Mahmoud et al [12].

Figure 22. Sample CMHB Used for Indirect Test Calibration

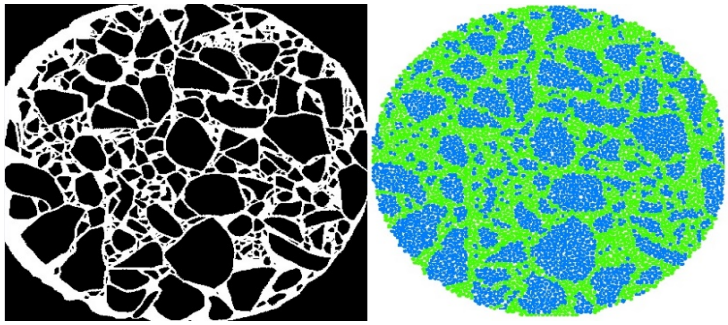

Figure 23. Sample Superpave Used for Indirect test Calibration

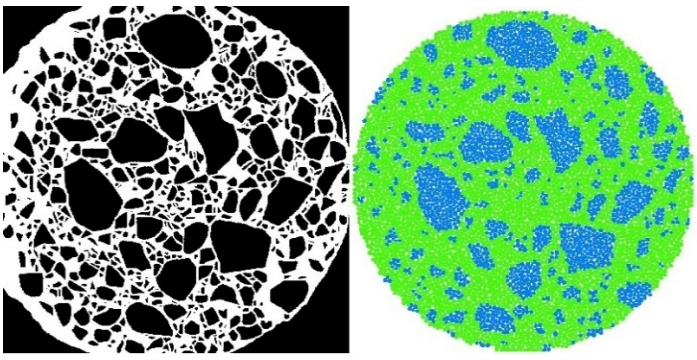

The following table was presented by Mahmoud et al. [12] as a comparison between the experimental and modelling results since the error percentage is negligeable. The adapted calibration results are valid and were adapted to conduct the sensitivity study in this report.

In order to save time and experimental expenses, the results of the calibration procedure were used to perform a similar indirect test conforming to the ASTM requirement instead of re-achieving the same procedure that was done twice already.

4.5 Support Conditions

The IDEAL-CT test represents a cylinder under tensile stress, aligned transversally, fixed at the bottom, and undergoing a force at the top. Multiple ways to fix the disk at the bottom are available within the software, either by introducing a fix wall or by fixing a few of the bottom balls. This second method was adapted; at a 19mm horizontal distance at the bottom of the disk, the balls were updated to be fixed throughout the simulation through the "fix" general command.

Figure 24. Support and Aggregate Balls Loading Rate

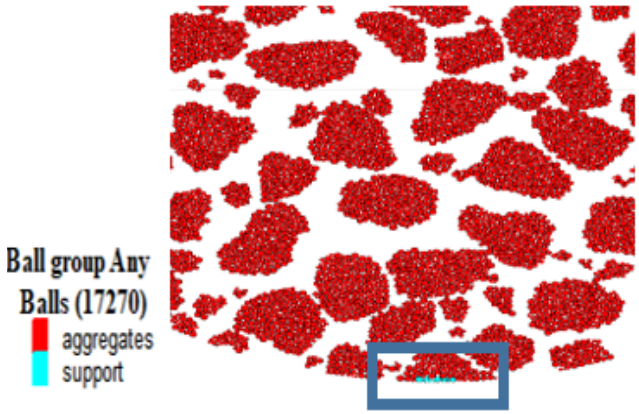

The loading rate a specimen can sustain in the laboratory is 50 mm/min, as per the ASTM's description [1]. However, the loading rate study conducted by Alvarado et al. [5], presented in the comparison below, shows that a loading rate greater than 2 in/s or the equivalent of 50 mm/s will yield a stress versus strain curve that is different than for a loading rate of 2 in/s. A lower loading rate yielded practically closer stress versus strain curves but would need greater computational time. The values in the analysis below are in inches per second.

Figure 25. Stress vs. Strain Curves for Different Loading Rates in an Indirect Tensile Test

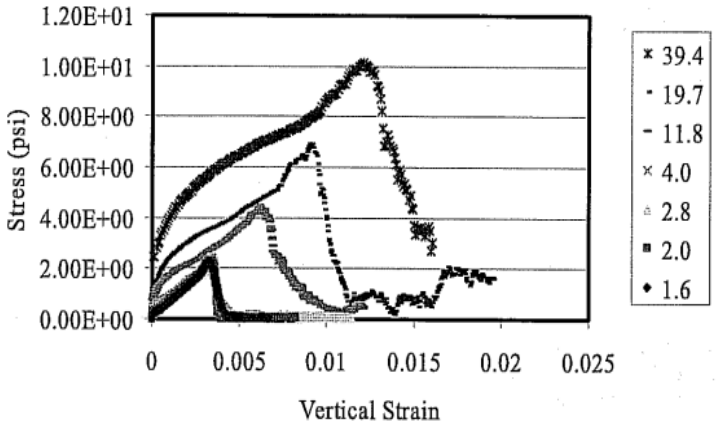

This comparison proves that 50 mm/s is the optimal choice for a loading rate since a greater loading rate would yield different results and a lower loading rate would result in simulation delays without considerable change in the behavior. Hence, it was decided to use 50 mm/s as the average loading rate with a range of ±2.5 mm/s.

The introduction of the load in the modelling procedure was done through the generation of a wall box at the top of the cylinder (Figure 26) and assigning the wall a downward velocity of the assigned loading rate for the exact model. While the wall starts moving downward, balls inside the cylinder start to move freely, and the contact bonds between the particles are triggered. Fractures start to appear up until the cylinder breaks and the simulation stops.

Figure 26. Sample Simulation

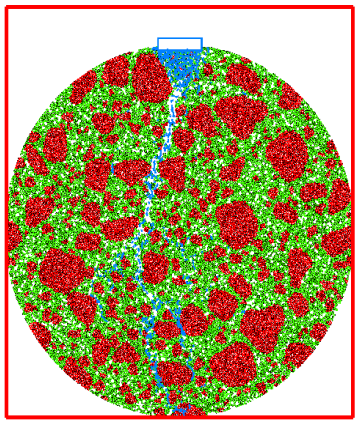

5. Results and Analysis

This study aims to demonstrate, through a sensitivity analysis, the responsiveness of the IDEAL-CT to changes in air void change and loading rate. Additionally, it aims to compare the behavior of low angularity aggregate versus high angularity aggregate mixes, using two different gradations: Superpave mix with 49% mastic and CMHB mix with less than 30% mastic. This is done with two different particle types: hard limestone and granite. For each scenario, around 20 random mixes were studied, leading to 100 simulations in each sensitivity study, 200 simulations for CMHB granite and hard limestone sensitivity comparison, 240 simulations for high angularity aggregate, and totaling over 400 overall simulations.

5.1 Load Displacement Curve Fitting

In order to compare the behavior between different scenarios and samples, the Cracking Tolerance index (CT) was computed for each simulation from its load versus displacement curve. The software draws the load versus displacement curve of each model through the "history" command, assigning the wall displacement values to the horizontal axis, and the wall contact forces to the vertical axis for each timestep of 10^{-7} seconds. The curve starts to develop when the wall starts moving downward until it reaches a maximum value, peak load, and then the load starts to decrease up until failure. The following figures show the load versus displacement curves of some high angularity aggregate mixes' output from the PFC2D software.

Figure 27. Load vs. Displacement Curve for CMHB Granite Samples

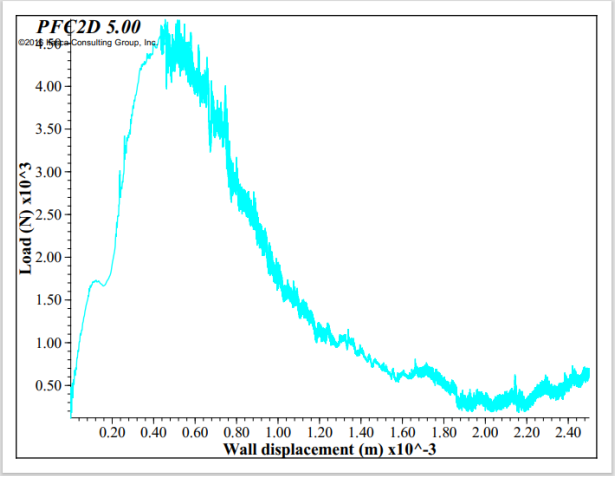

Figure 28. Load vs. Displacement Curve for Hard Limestone Samples

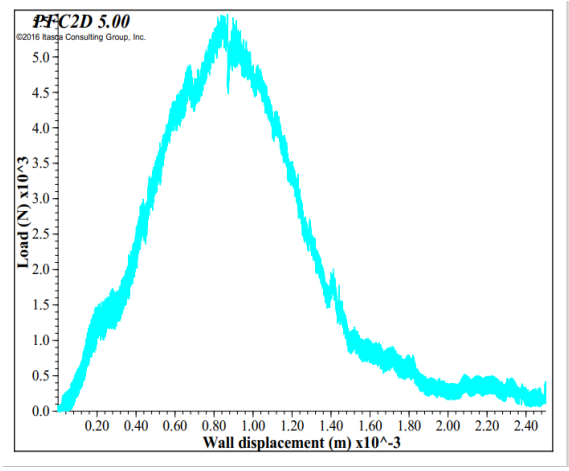

Figure 29. Load vs. Displacement Curve for CMHB Granite Samples

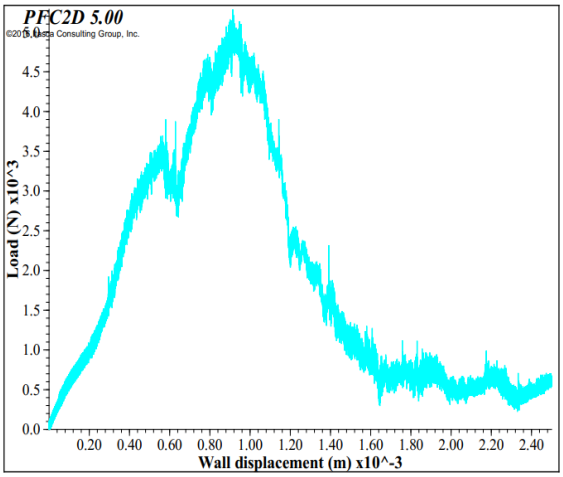

Figure 30. Load vs. Displacement Curve for Hard Limestone Samples

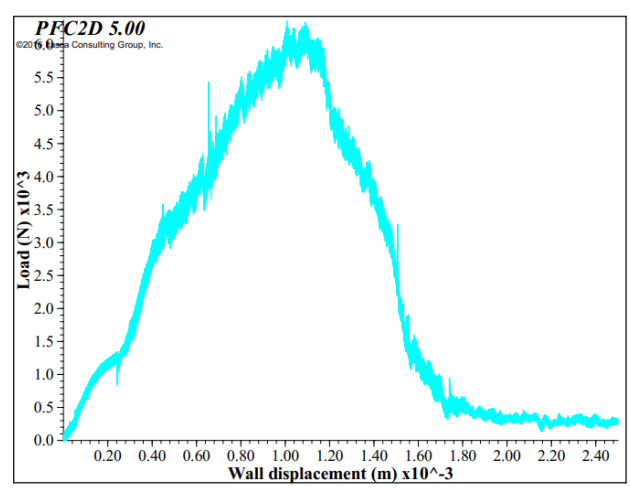

The result of each simulation was imported into Microsoft Excel, and each graph was then analyzed. During the laboratory test, as the specimen is subjected to a constant load, the resulting load-displacement curve can be generated and observed simultaneously, that is, in real time. Whenever the load drops below 100 N, the simulation stops as per ASTM publications [1]. Therefore, the same analysis is conducted while studying each load-displacement curve. The last part of the graph represents values after the cylinder breaks; hence it can be disregarded.

For the purpose of adequately computing the CT index for each sample, a curve regression is indispensable. An iteration of 1st order to 4th order regression was made, and the choice of using the 4th order regression resides in the fact that the data were found to follow a 4th order polynomial distribution. By employing this high order of regression, the model can more accurately capture the complex relationships within the data, thereby improving the accuracy of the computed CT index. A quick statistical screening for the plots shows that a 4th order of regression yields a closer match to the existing curve, a small margin of error, and a coefficient of determination close to 1. The following load displacement presents the regression of Figures 27, 28, 29, and 30 above. These curves show both the original curve and its regression, and the equation of each is shown on the curve alongside the R^2 values. As shown in the figures below, the fitting is considered acceptable for R^2 values greater than 0.9, and the regressed curves are then used for further analysis.

Figure 31. Load Displacement Curve for CMHB-Hard Limestone

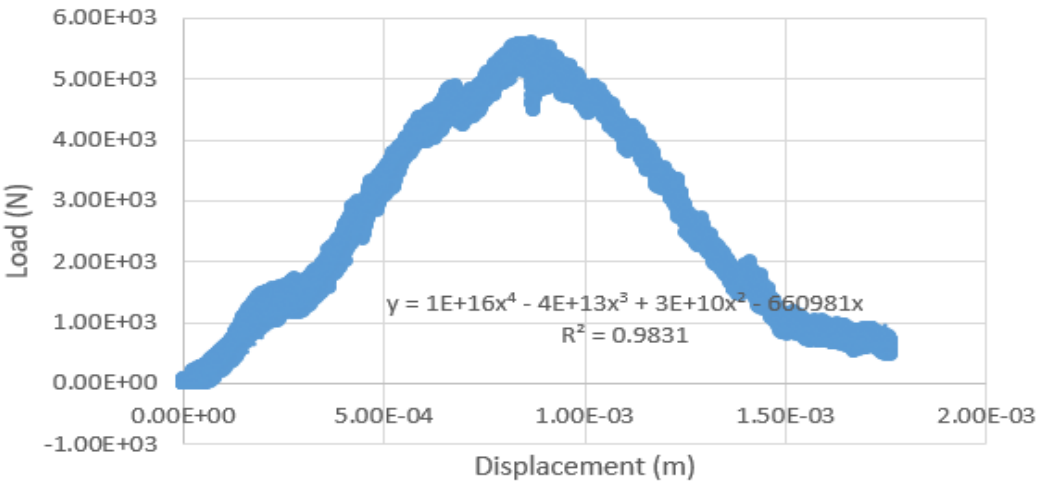

Figure 32. Load Displacement Curve for CMHB-Granite

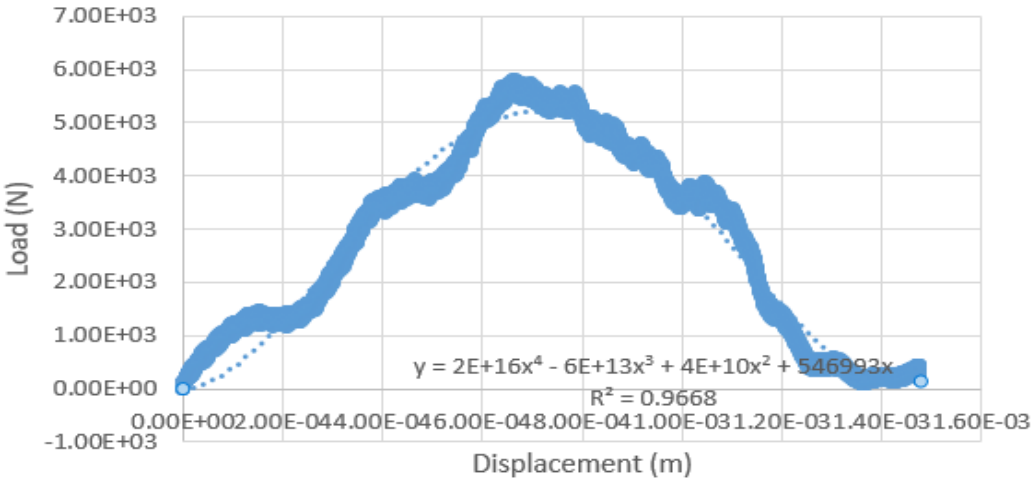

Figure 33. Load Displacement Curve for Superpave-Granite

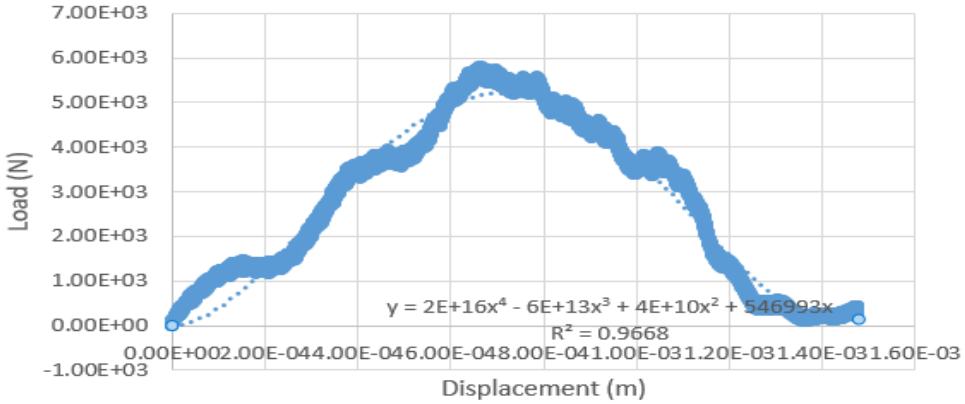

Figure 34. Load Displacement Curve for Superpave-Hard Limestone

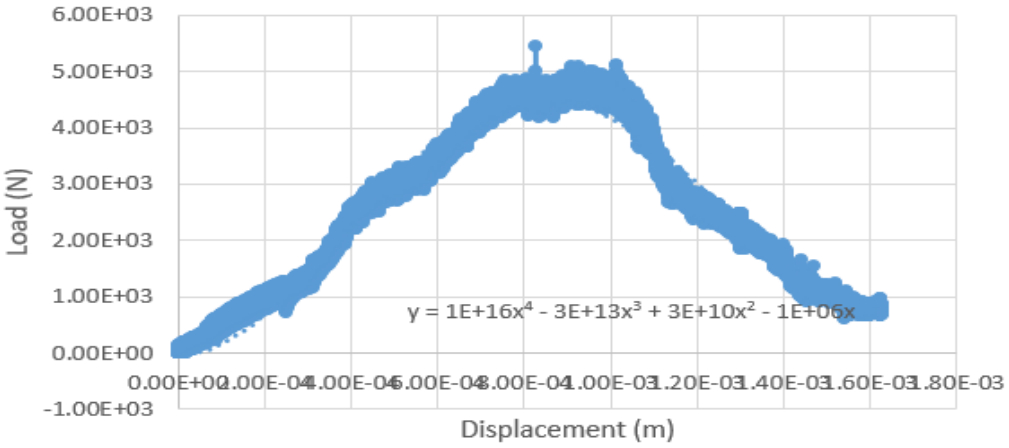

5.2 Fracture Development

The crack development procedure can also be observed in PFC2D software through the discrete fracture network (DFN) module. This model describes cracks as line segments in 2D, and cracks are limited inside the model domain and can appear in between particles. Once the simulation starts, fractures start to develop underneath the wall body at the top and near the support balls at the bottom. Then, DFN segments connect through the voids first. At that point, whenever the contact bond between asphalt bodies breaks, fractures start to develop between mastic bodies, then between aggregate and mastic. A few cracks develop between aggregate particles, and the connection of the fractures breaks the cylinder. The following pictures describe the development of the DFN during simulation for a CMHB granite sample.

Figure 35. Crack Development Process

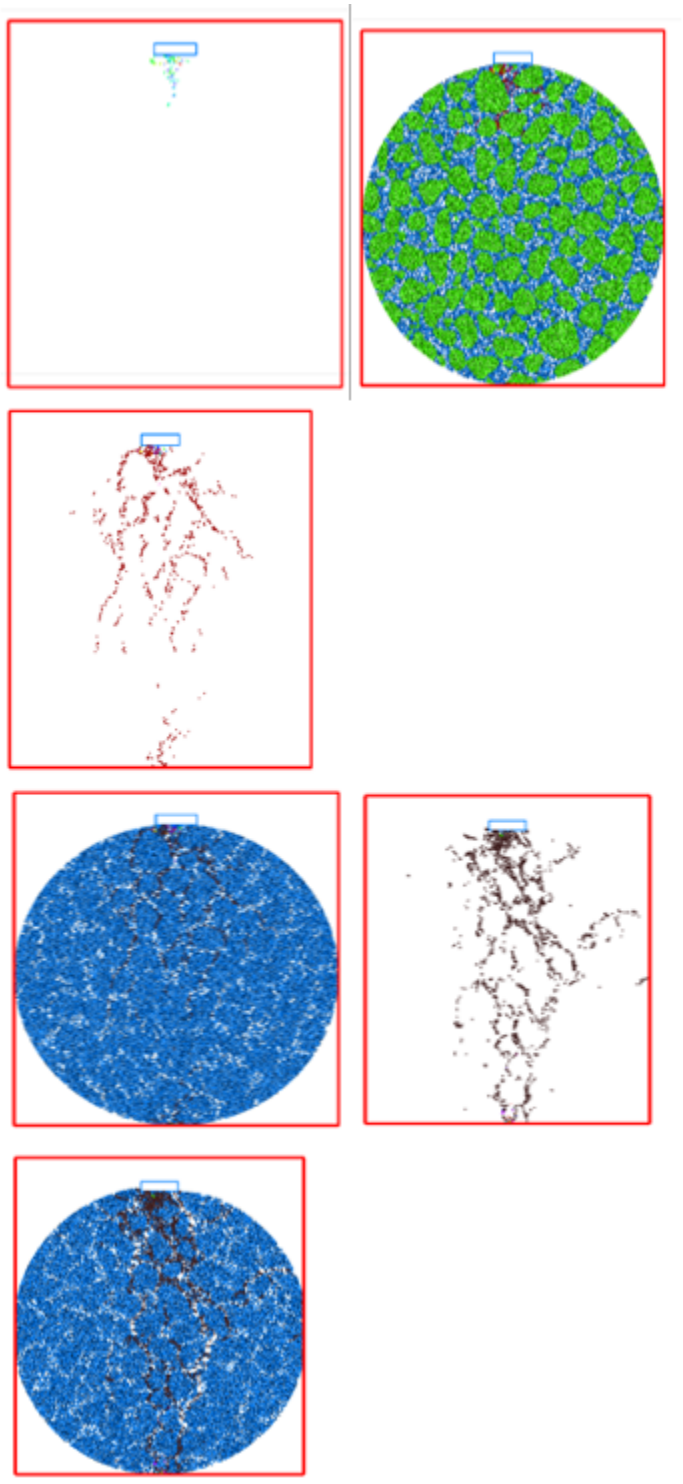

The failure of the cylinder shape, whether the cylinder breaks in half or breaks from the top, depends mostly on the distribution of the voids since the majority of DFN modules develop and connect through the voids. The following figures show the development of cracks for different samples of different mixes.

Figure 36. Example Fractures in CMHB Mixes

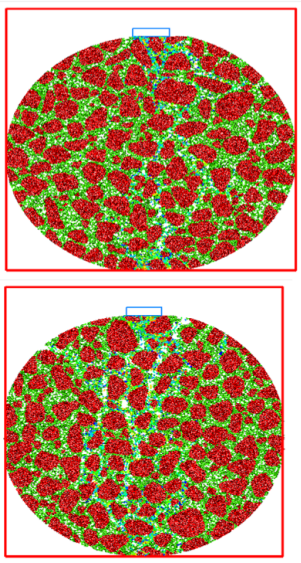

Figure 37. Example Fractures in Superpave Mixes

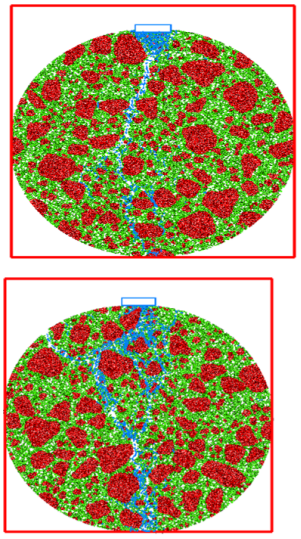

5.3 Cracking Tolerance Calculation

The ability to quantify cracking tolerance is one of the innovations of the IDEAL-CT. This is done through a unique index that can uniformly compare the cracking resistance of any given mix through its load-displacement curve. The CT index depends on the failure energy of the specimen, the post-peak slope, and the deformation tolerance at 75% of the peak load. Since this report pivots around sensitivity analysis and mix comparisons, the CT index was calculated for every sample type. The following curve and series of equations was applied to every mix in order to calculate the CT index. Usually, the better the cracking resistance the higher the CT index. The following curves underline the factors used for the calculation: peak value, 75% of peak value, post peak slope

using load at 65% and 85% after the peak load, and the displacement when 75% of the load is dissipated. Also, the cracking resistance depends on the failure energy, which is the work of failure divided by the cross-sectional area of the specimen. The work of failure is equal to the area under the load-displacement curves.

Figure 38. Load Displacement Curve for CT index Calculation

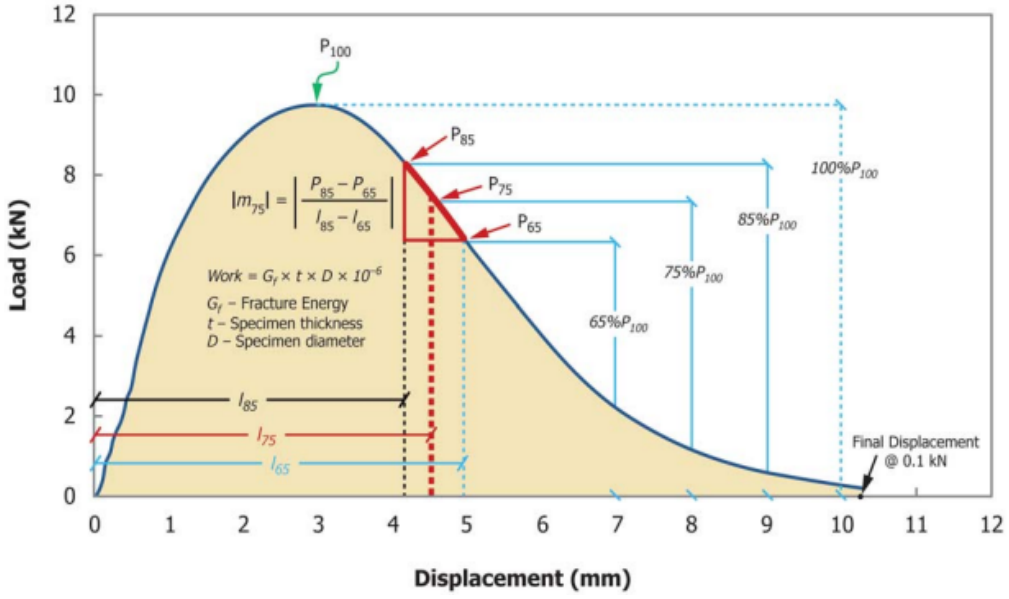

The calculation of each index is as follows:

$$CT_{index} = \frac{t}{62} \times \frac{l_{75}}{D} \times \frac{G_f}{|m_{75}|} \times 10^6$$

With:

- t: specimen thickness considered 62 mm
- l_{75}: displacement at 75% of the peak load after the peak (mm)
- D: specimen diameter (mm) taken equal to 150 mm
- $|m_{75}|$: absolute value of the post-peak load slope (N/m)
- G_f: failure energy (Joules/m^2)

The work of failure is calculated by dividing the area under the load displacement curve by the cross-sectional area of the specimen [1] following the formula below:

- $G_f = \frac{W_f}{D \times t} \times 10^6$
- W_f: work of failure (Joules) calculated as the area under the load displacement curve.
- $\frac{t}{62}$: is a unitless correction factor for specimen thickness, considered a unit in this analysis.

Following the procedure explained above, the CT index was computed, and the results are summarized below.

5.4 CT index for High Angularity CMHB Granite Samples

The calculation of the CT index was done for 20 different mixes for each scenario (refer to Table 1 for scenario descriptions). The load displacement curve was studied for every mix. The peak load was evaluated, then the post peak slope, the work of failure, and failure energy were computed and compared between mixes. The following table summarizes the calculation procedure for the CMHB-Granite mix with 7% air void content and a loading rate of 0.05 m/s.

Table 9. Calculation of the CT index for CMHB-Granite

7% AV-Loading 0.05					
	Peak Load	**I75 (mm)**	**Gf (Joules)**	**m_{75}**	**CT index**
Mix 1	4.50	1.25	700.04	2812500.00	2.10
Mix 2	3.10	0.70	1752.69	4133333.33	2.00
Mix 3	4.00	0.82	4620.30	11428571.43	2.20
Mix 4	3.95	0.78	343.02	7181818.18	2.20
Mix 5	3.20	0.82	1820.12	4266666.67	2.30
Mix 6	4.00	0.82	3780.24	8000000.00	2.60
Mix 7	4.20	0.78	4620.30	10500000.00	2.30
Mix 8	4.00	0.75	4620.30	4444444.44	2.40
Mix 9	3.90	0.75	4620.30	7090909.09	3.30
Mix 10	4.20	1.15	1820.12	3360000.00	2.50
Mix 11	5.10	0.92	4620.30	10200000.00	2.80
Mix 12	3.70	1.05	3220.21	3700000.00	2.20
Mix 13	4.00	0.75	3080.20	6153846.15	2.50
Mix 14	4.00	0.75	3080.20	6153846.15	2.50
Mix 15	4.75	1.25	560.04	2111111.11	2.20
Mix 16	4.00	0.78	4620.30	10000000.00	2.40
Mix 17	2.50	0.60	4395.96	7142857.14	2.50
Mix 18	3.50	1.20	212.19	2333333.33	2.20
Mix 19	4.00	0.75	3080.20	6153846.15	2.50
Mix 20	3.50	0.80	235.48	4666666.67	2.10

The same procedure was repeated for two different 6% air void samples and 8% air void samples with different loading rates. Two values were evaluated for each mix: the peak load and the CT index. The graphs below summarize the findings for the CMHB-granite mixtures. Scenarios 1 and 2 refer to the 6% air void mixes, with 0.0475 m/s and 0.0525 m/s loading rates, respectively, and Scenarios 3 and 4 refer to the 8% air void mixes with 0.0475 m/s and 0.0525 m/s loading rates, respectively.

Figure 39. Probability Plot for Peak Load for Different Mixes of CMHB-Granite

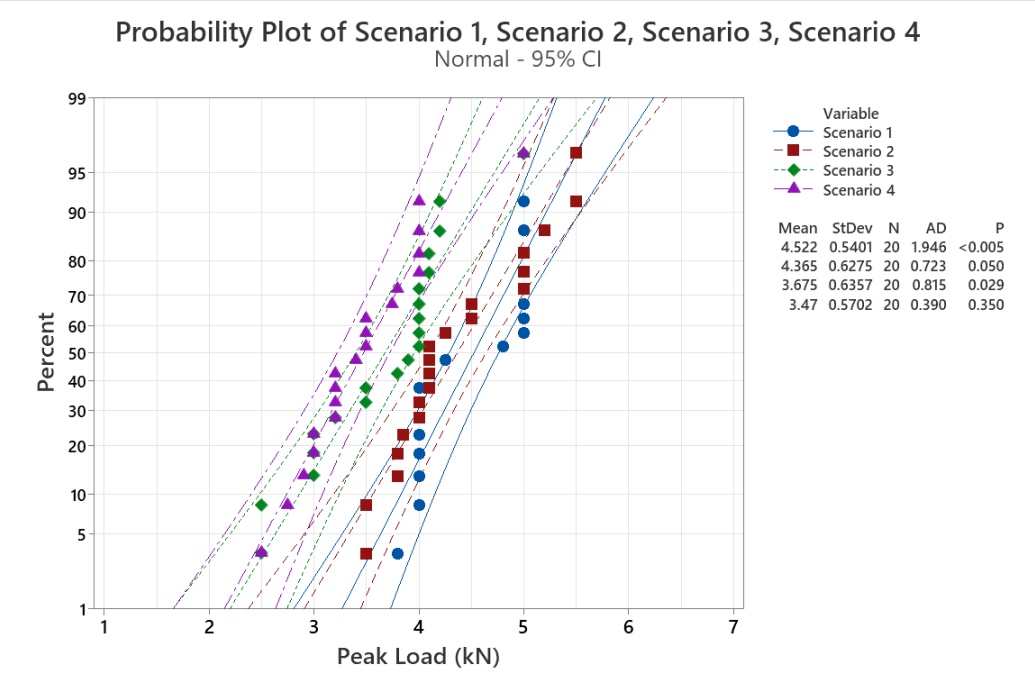

First, a quick screening of the peak load values shows a considerable difference between Scenarios 1 and 2 on the one hand and Scenarios 3 and 4 on the other. The 8% air void mixes (Scenarios 3 and 4) break at a peak value between 3 and 4 KN, while the 6% air void mixes withstand a greater load, up to 5 and 6 KN. This difference shows that a change of 2% in air void content would yield a difference of around 20%. Hence, air void percentage has a great impact on the peak load a mix can withstand before breaking.

In another instance, the difference in the peak load between mixes 1 and 2 for samples with the same air void content and different loading rates is imperceptible in the graph above. However, the average standard deviation and coefficient of variance were computed for the peak load of the samples in each scenario and the results are below.

Table 10. Peak Load Statistical Analysis for Different Mixes of CMHB-Granite

Peak load				
	Scenario 1	Scenario 2	Scenario 3	Scenario 4
Mix 1	5	5	3	2.9
Mix 2	4.8	3.8	3.5	3.2
Mix 3	5	5.5	5	5
Mix 4	5	3.8	4	4
Mix 5	5.5	5	4	3.75
Mix 6	4	5.2	3.5	3.4
Mix 7	4	3.5	3.8	3.5
Mix 8	5	5.5	4.2	2.5
Mix 9	3.8	4.5	4.2	3.5
Mix 10	4	4	2.5	4
Mix 11	4.25	3.85	3.9	3.5
Mix 12	4.1	4.25	4	4
Mix 13	4	3.5	4	3.2
Mix 14	4	4.5	3.2	3
Mix 15	5	4.1	4.1	4
Mix 16	5	4.1	4.1	3
Mix 17	4	4.1	4	2.75
Mix 18	5	4.1	3	3.8
Mix 19	5	5	3	3.2
Mix 20	4	4	2.5	3.2
Mean	4.5225	4.365	3.675	3.47
STDDEV	0.526421	0.611576	0.619576468	0.56
COV	11.64004	14.0109	16.85922363	16.02

The table above shows the average values of peak load for each mix, proving that a decrease in air void percentage would yield an increase of around 20% in peak load values. Moreover, a decrease of 0.05 m/s in air void yielded an increase of 3% in peak load values for the 6% air void mixes and an increase of 6% for the 8% air void mixes. Hence, both air voids and loading rates have a negative impact on the peak load value of a mix in indirect tensile conditions, and any increase in these factors would result in a decrease in peak load values. Furthermore, the coefficient of variation (COV) is computed for the 20 mixes withstanding the indirect tensile tests. This coefficient of variation index is calculated for the purpose of evaluating the distribution of the values around the mean. These tests presented a COV of less than 20%. Therefore, the random distribution of particles in the software gave reasonable results statistic-wise. Hence, this test can be considered repeatable. However, since the peak load is not the only variable able to describe the cracking

resistance of the samples, the comparison was also conducted for the samples' CT index as shown in the graph below.

Figure 40. Probability Plot for the CT index of Different Mixes of CMHB-Granite

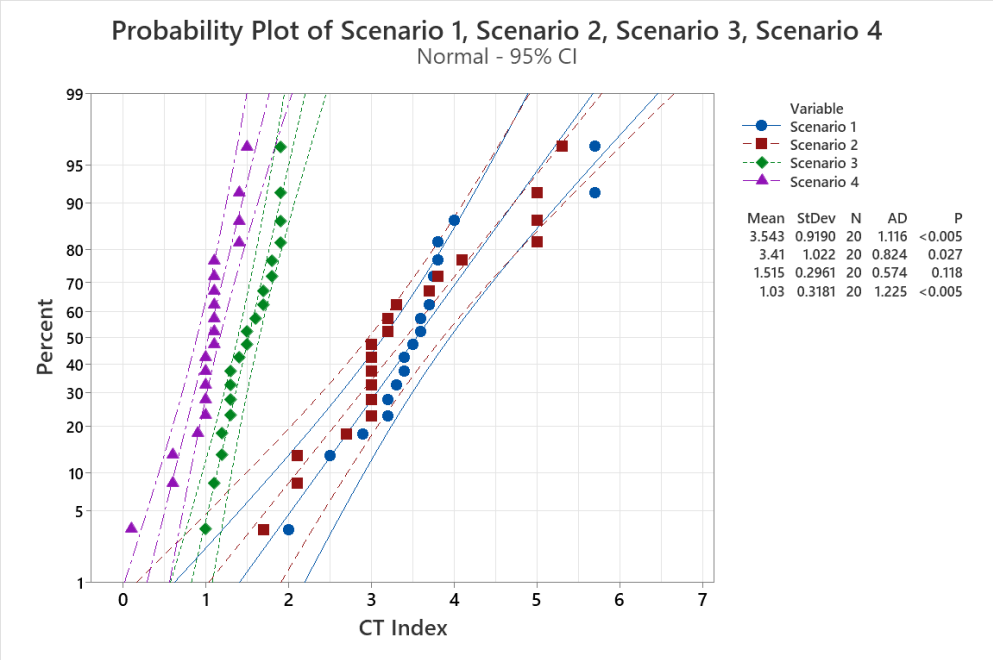

The CT index for samples with 8% air voids can go as low as 1 and 2, while 6% air void samples have a higher CT index that can range around 3 and 4 with a few exceptions that can reach 5, as shown above. Also, the difference between Scenarios 1 and 2 is small, with the samples undergoing lower loading rates yielding slightly greater CT index values. The same can be said about Scenarios 3 and 4, where scenario 3 (0.0475 m/s) showed slightly greater CT index values. The statistical analysis of the samples and the variation is presented in the table below:

Table 11. CT index Statistical Analysis for Different Mixes of CMHB-Granite

	CMHB-Granite-CT index Calculation			
	Scenario 1	Scenario 2	Scenario 3	Scenario 4
Mean	3.54	3.41	1.52	1.03
STD DEV	0.90	1.00	0.29	0.31
COV (%)	25.29	29.21	19.05	30.10

The average CT index shows a decline of more than 50% for a 2% increase in air voids, while a decrease in 0.05 m/s resulted in a smaller increase in CT index values. Coefficients of variation values do not exceed 30%, thus the CT index calculation can also be considered as repeatable for the 20 mixes in question. Since the values for Scenarios 1 and 2 and Scenarios 3 and 4 are close for

both peak loads and CT index calculation, a further statistical study was conducted using the T-method of statistical analysis assuming both mean distributions are equal. The following tables represent the peak load T-test distribution followed by the CT index T-tests as well.

Table 12. T-Test for Peak Load for Scenarios 1 and 2

	Scenario 1	*Scenario 2*
Mean	4.5225	4.365
Variance	0.291704	0.393710526
Observations	20	20
Df	38	
P(T<=t) two-tail	0.400219	
t Critical two-tail	2.024394	

Table 13. T-Test for Peak Load for Scenarios 3 and 4

	Scenario 3	*Scenario 4*
Mean	3.675	3.47
Variance	0.404079	0.325105263
Observations	20	20
Df	38	
P(T<=t) two-tail	0.289764	
t Critical two-tail	2.024394	

Table 14. T-Test for CT index for Scenarios 1 and 2

	Scenario 1	*Scenario 2*
Mean	3.5425	3.41
Variance	0.844546053	1.044105
Observations	20	20
Df	38	
P(T<=t) two-tail	0.668776369	
t Critical two-tail	2.024394164	

Table 15. T-Test for CT index for Scenarios 3 and 4

	Scenario 3	*Scenario 4*
Mean	1.515	1.03
Variance	0.087657895	0.101157895
Observations	20	20
Df	38	
P(T<=t) two-tail	1.36304E-05	
t Critical two-tail	2.024394164	

The T-test conducted on these variables shows a P-value between Scenario 1 and 2 greater than alpha or a confidence interval equal to 5%, hence it cannot be assumed that the two CT indexes for Scenarios 1 and 2 are different on a level of confidence of 95%. Thus, even if a higher loading rate yielded greater peak load and a greater CT index, it cannot be concluded that this difference is statistically significant.

5.5 CT Index for High Angularity CMHB Hard Limestone Samples

Figure 41. Probability Plot for Peak Load for Different Mixes of CMHB-Hard Limestone

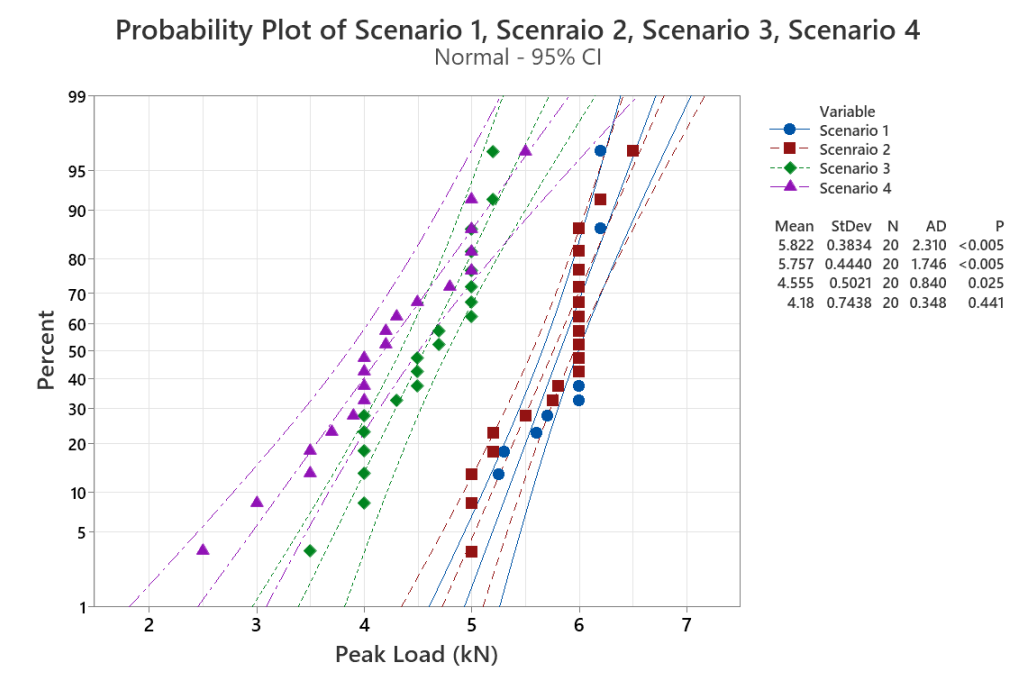

The same analysis was conducted for CMHB hard limestone mixes: the peak load is evaluated for the 20 samples in each scenario. The mixes with 8% air voids presented a peak load value of 4 to 5 KN while mixes with 6% air voids withstand 6 KN before breaking. Samples under a greater

loading rate also withstand slightly lower peak load values, and the following statistical study shows that the peak load analysis for the mixes in question have a low coefficient of variation and can indeed be considered as repeatable.

Table 16. CT Index Statistical Analysis for Different Mixes of CMHB-Hard Limestone

Peak Load-CMHB-HL				
	Scenario 1	Scenario 2	Scenario 3	Scenario 4
Mean	5.82	5.76	4.56	4.18
SD	0.37	0.43	0.49	0.72
COV (%)	6.42	7.52	10.74	17.34

Figure 42. Probability Plot for CT index for Different Mixes of CMHB-Hard Limestone

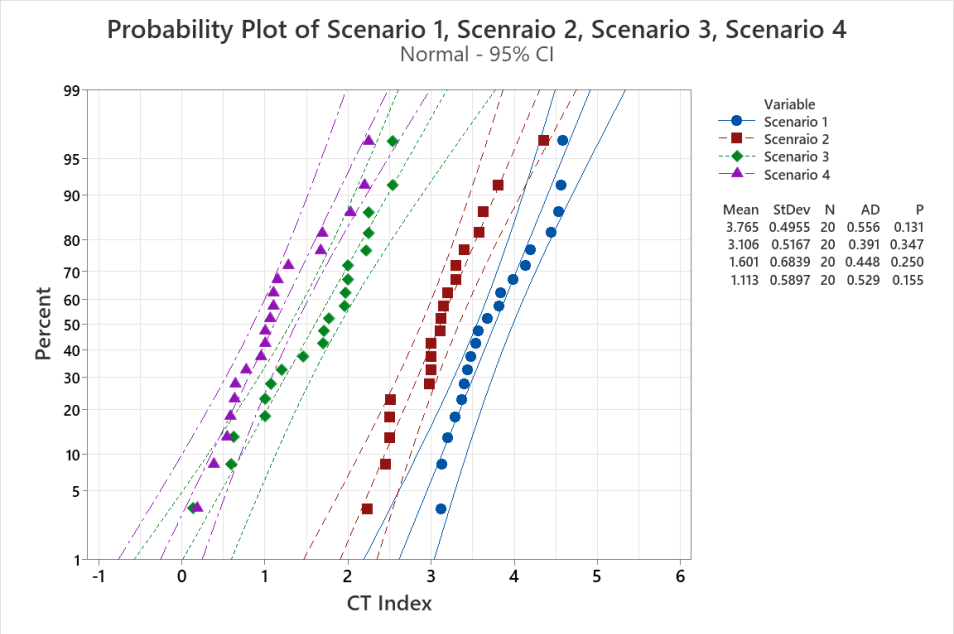

Also, the calculation of the CT index shows a remarkable difference between 8% air void samples with CT indexes ranging from 1 to 2.5, while 6% air void samples show greater values between 3 and 4.5. Additionally, mixes with greater loading rates have slightly less CT index values. Since the values for scenarios with the same air void content are close, the T-test was also conducted for both peak value and CT index calculations for Scenarios 1 and 2, as well as Scenarios 3 and 4. The following table shows the peak value for the T-test for Scenarios 3 and 4; a greater peak value proves that there is not a significant difference between the behaviors of these two scenarios.

Table 17. T-Test for CT index Scenarios 3 and 4

	Scenario 3	Scenario 4
Mean	1.601025103	1.112615731
Variance	0.467681243	0.347769533
Observations	20	20
df	38	
P(T<=t) two-tail	0.02046939	
t Critical two-tail	2.024394164	

To conclude, the IDEAL-CT performed in the PFC2D software is sensitive to air void variation. This factor has a negative impact on the cracking resistance of the mix, while air voids are far more impactful than the loading rate, which did not yield a statistically significant change in behavior. These tests have proven to have a low coefficient of variation and can thus be considered repeatable.

5.6 CT index and Peak Load for Different Mixes of High Angularity

After completing the sensitivity analysis of the IDEAL-CT, tests on samples with 7% air void content and undergoing a constant loading rate of 0.05 m/s were conducted to compare granite, hard limestone material, Superpave, and CMHB gradation. A total of 20 samples were presented for each mix type, and then the comparison between peak load and CT indexes was established.

5.6.1 Granite and Hard Limestone

Figure 43. Probability Plot for Peak Load for CMHB Mixtures for both Granite and Hard Limestone

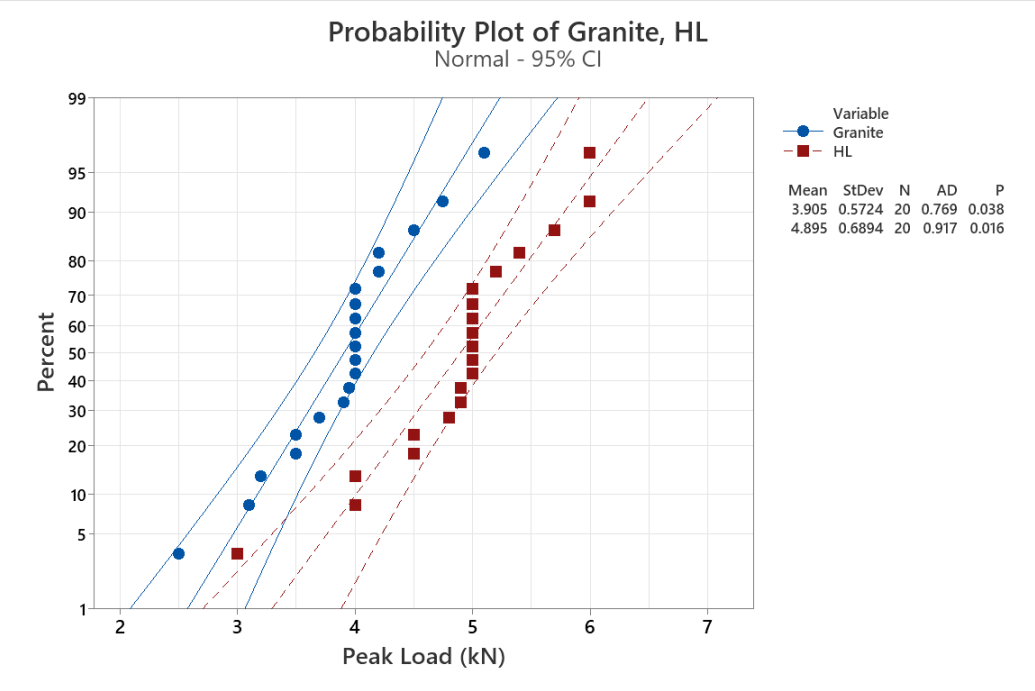

Figure 44. Probability Plot for Peak Load for Superpave Mixtures for both Granite and Hard Limestone

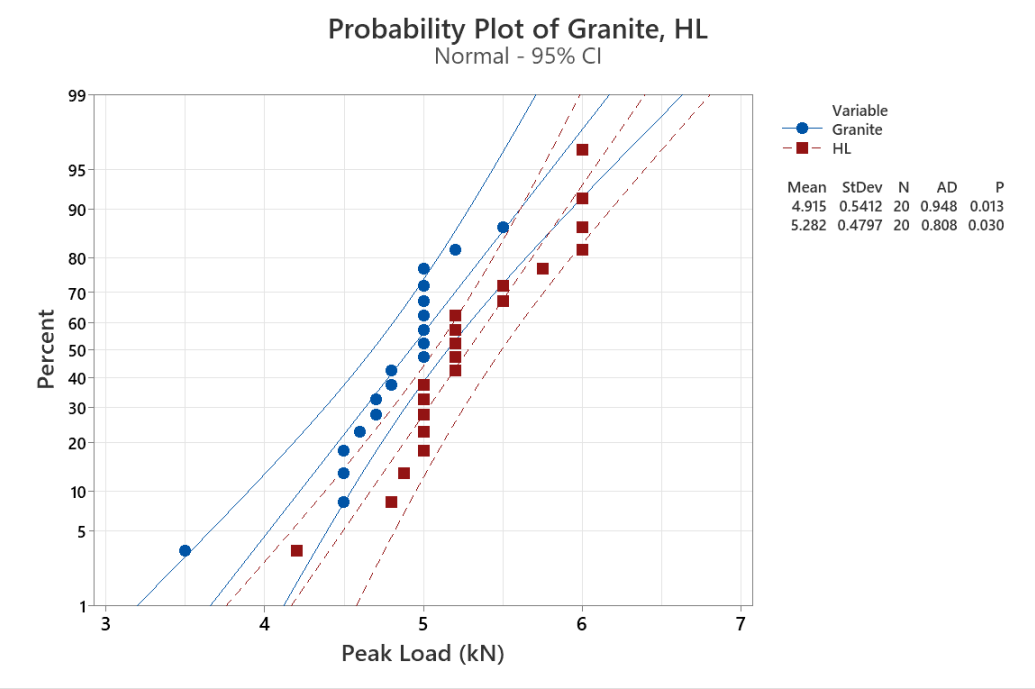

Both mixture gradations show that hard limestone can resist a greater load before breaking than granite material. While hard limestone can withstand up to 6 KN before breaking, granite can break under a 4 KN peak load.

Figure 45. Probability Plot for CT index for CMHB Mixtures for Both Granite and Hard Limestone

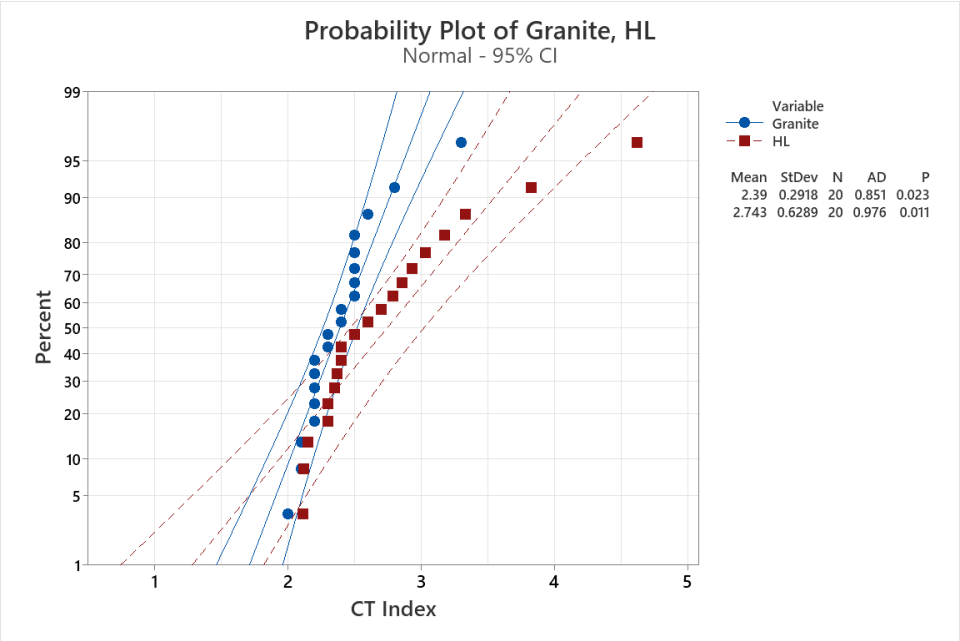

For CMHB mixtures, hard limestone samples have a CT index greater than 3 while granite's CT index hovers around 2. Tensile strength for granite aggregates is slightly greater than the tensile strength assigned for hard limestone aggregates, while asphalt tensile strength is 10 times greater for hard limestone than granite. Thus, for CMHB gradation, the cracking behavior is mostly dictated by the asphalt, and hard limestone presents higher cracking resistance than granite. On the other hand, the figure below shows the distribution of CT index for Superpave mixtures comparing granite and hard limestone material. Some of the granite samples have greater CT indexes than hard limestone and vice versa, and no general comparison can be deduced from comparing the mixes in general. Hence, the average values can be compared instead.

Figure 46. Probability Plot for CT index for Superpave Mixtures for both Granite and Hard Limestone

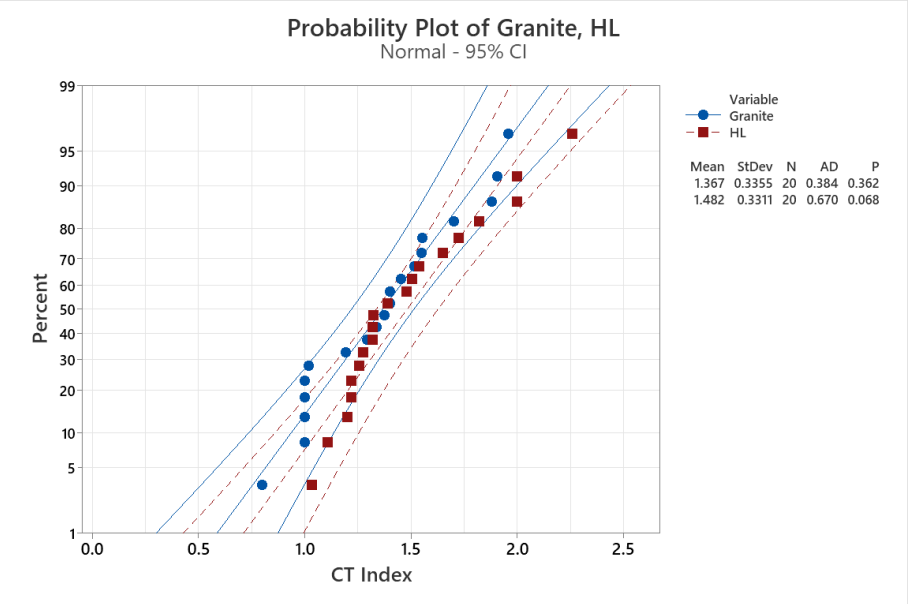

For Superpave mixes, the average CT index for HL is slightly greater than the average CT index for granite, and the same goes for CMHB mixtures. Thus, hard limestone performs better in cracking resistance than granite due to the greater tensile strength between the mastic particles for hard limestone samples.

5.6.2 CMHB versus Superpave

First, the graph below shows a greater peak load value for the Superpave mix gradation than the CMHB mix gradation. CMHB samples resist loads of less than 5 KN while Superpave mixtures resist up to 6 KN before breaking.

Figure 47. Probability Plot for Peak Load Comparison for Granite Mixtures for both Superpave and CMHB Gradations

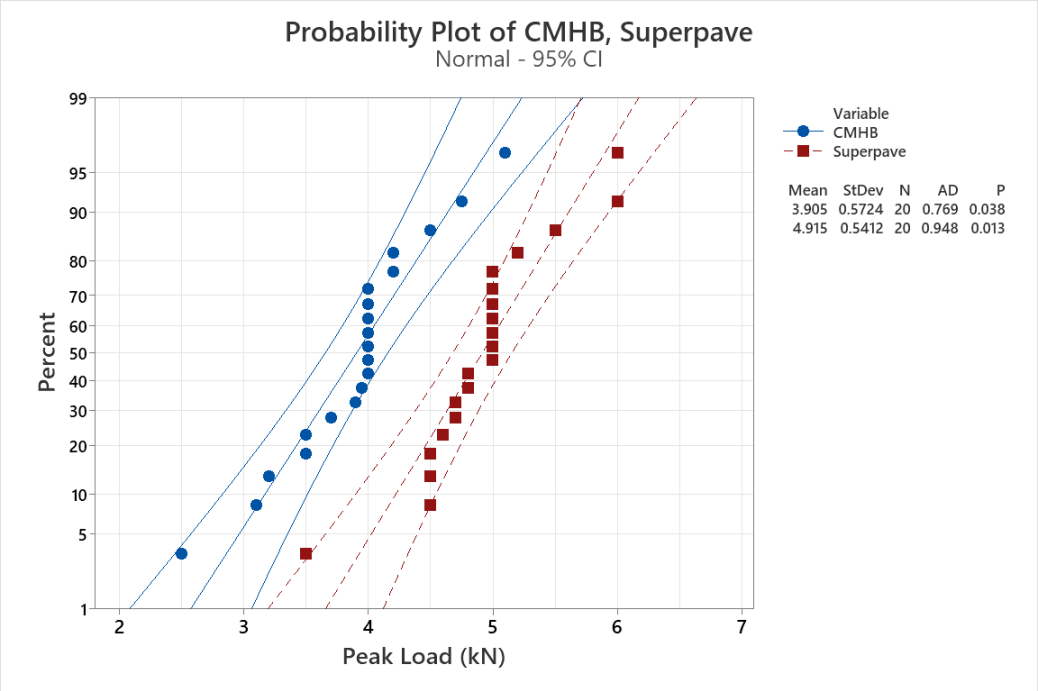

On the other hand, the CT index correlations (Figure 48) shows that CMHB gradation better resists cracking. Even though it breaks under a smaller load, it has greater CT index values—between 2 and 3—while Superpave gradation presents a CT index lower than 2.

Figure 48. Probability Plot for CT index Comparison for Granite Mixtures for both Superpave and CMHB Gradations

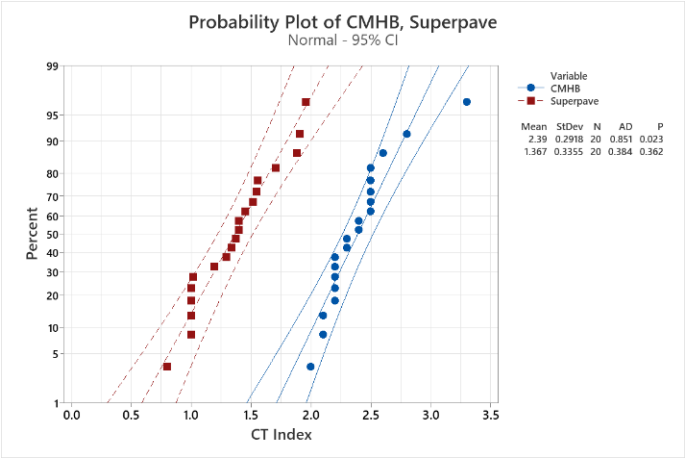

The same study was also conducted for hard limestone samples, and the figures below present the peak load and CT index comparison for both gradations.

Figure 49. Probability Plot for Peak Load Comparison for HL Mixtures for both Superpave and CMHB Gradations

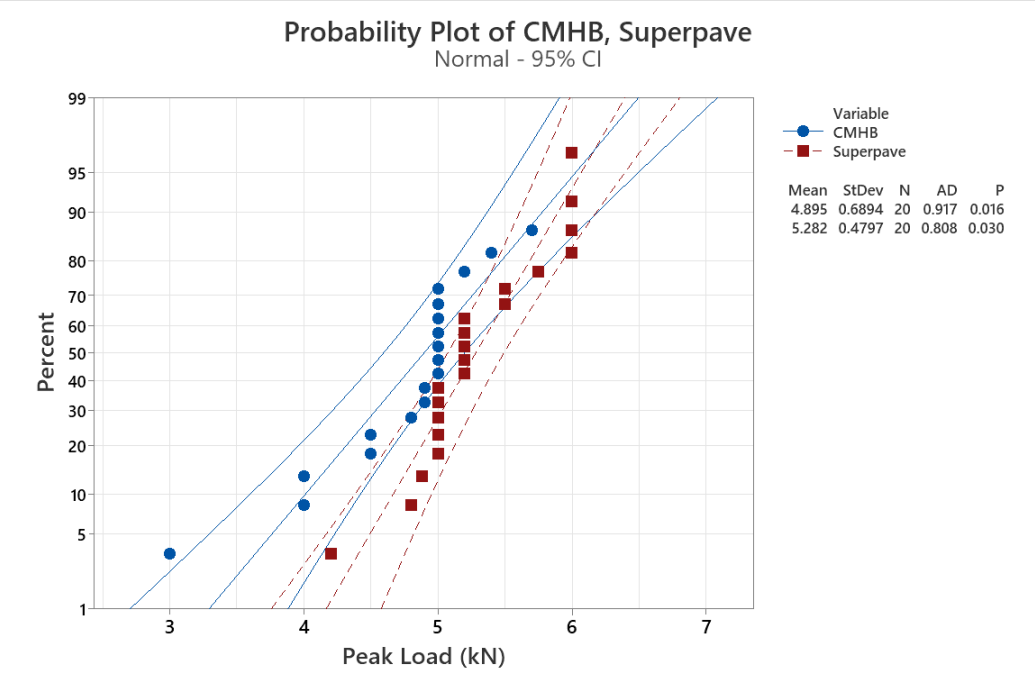

Figure 50. Probability Plot for CT index Comparison for HL Mixtures for both Superpave and CMHB Gradations

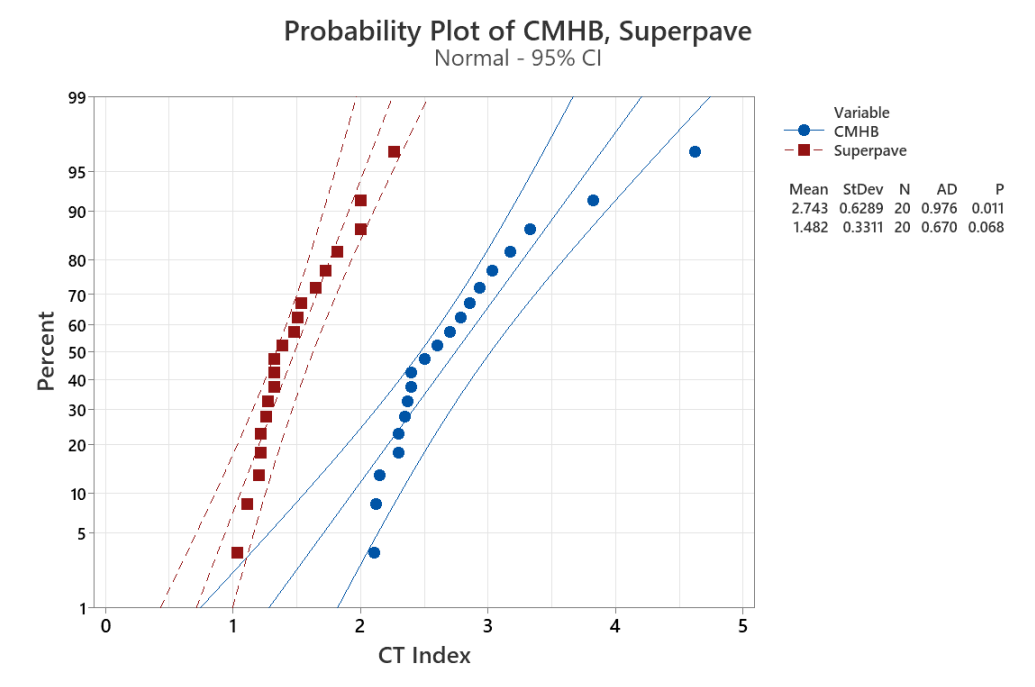

Both materials present the same behavior for different gradations; Superpave gradation can resist a greater peak load before breaking, while CMHB gradation is more resistant to cracking.

5.7 CT Index and Peak Load Comparison between High Angularity and Low Angularity Aggregates

For the purpose of comparing the impact of aggregate angularity and shape on the cracking behavior, more than 20 random samples were generated for CMHB granite, another 20 for CMHB hard limestone, as well as another 40 for Superpave gradation, and every mix type with low angularity aggregates was compared to the similar mix with high angularity aggregates. After that, the peak load of every mix's type was compared to the previous findings, as well as the CT index analysis. The following figures summarize the analysis.

Figure 51. Probability Plot for Peak Load Comparison for CMHB-Granite Mixes for both High and Low Angularities

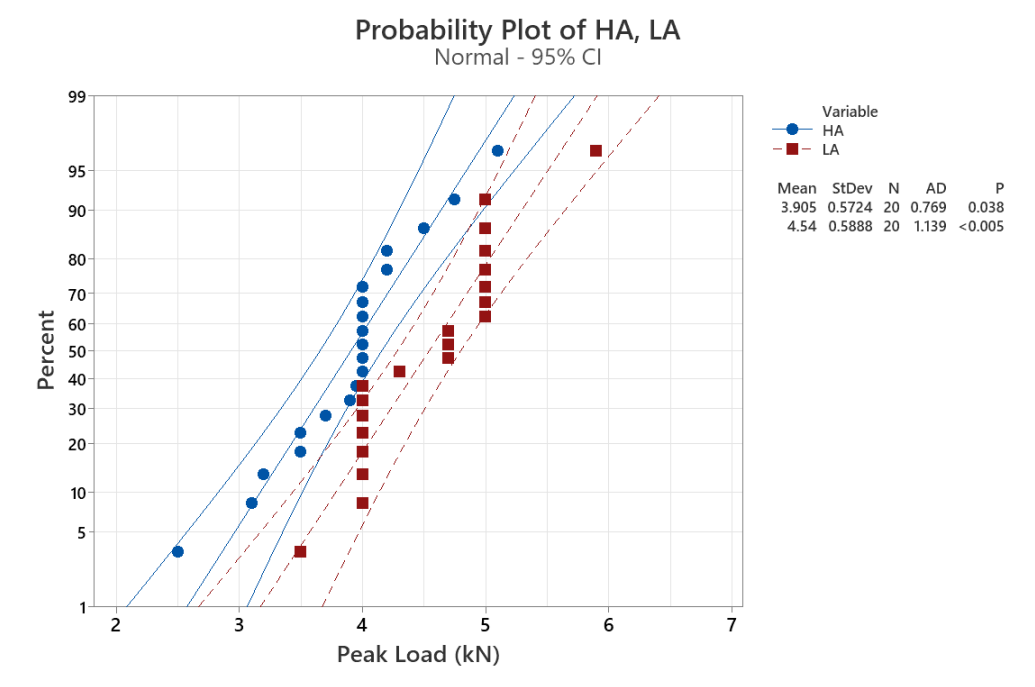

Figure 52. Probability Plot for CT Index Comparison for CMHB-Granite Mixes for both High and Low Angularities

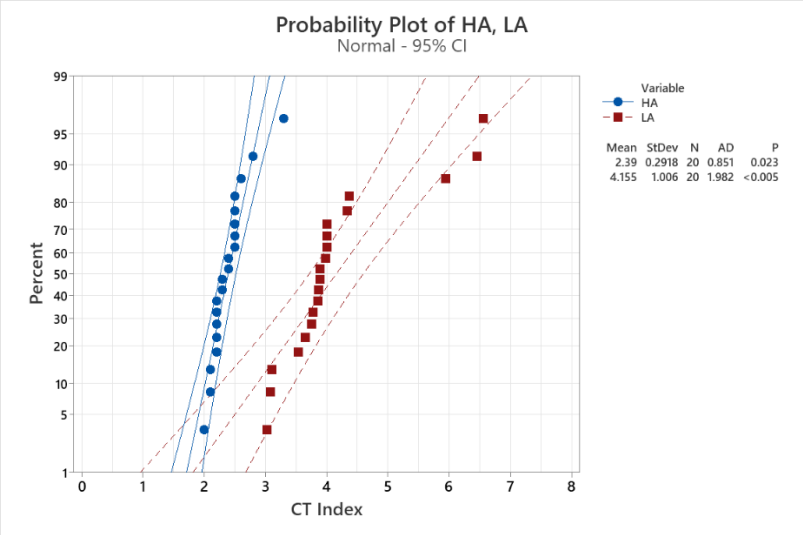

Figure 53. Probability Plot Comparison for Peak Load for CMHB-HL Mixes for both High and Low Angularities

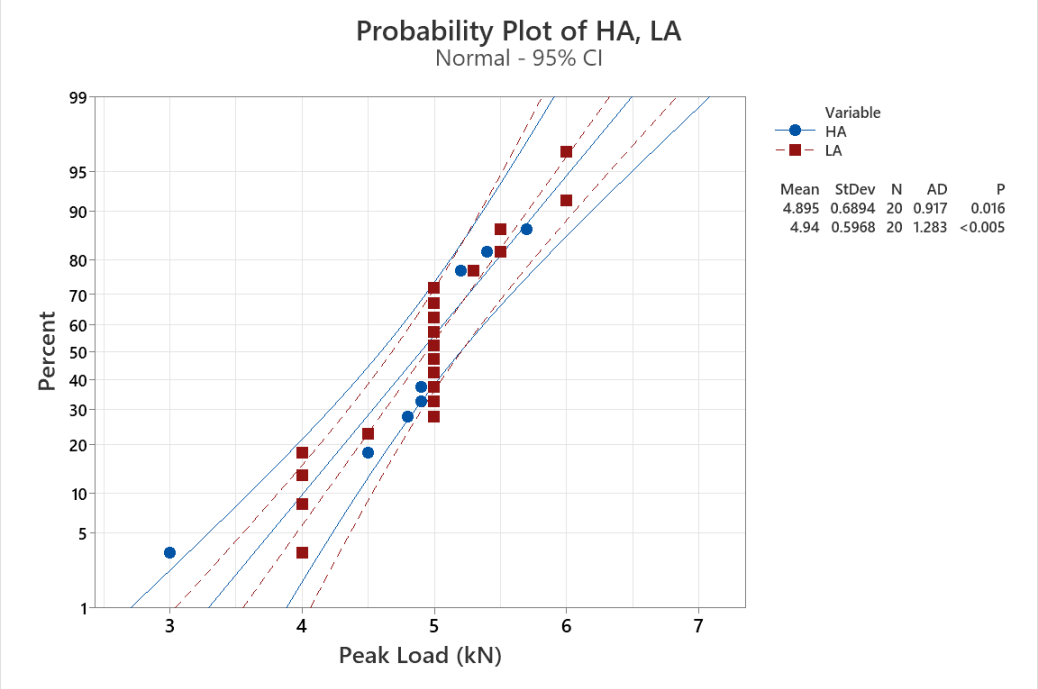

Figure 54. Probability Plot for CT Index Comparison for CMHB-HL for both High and Low Angularities

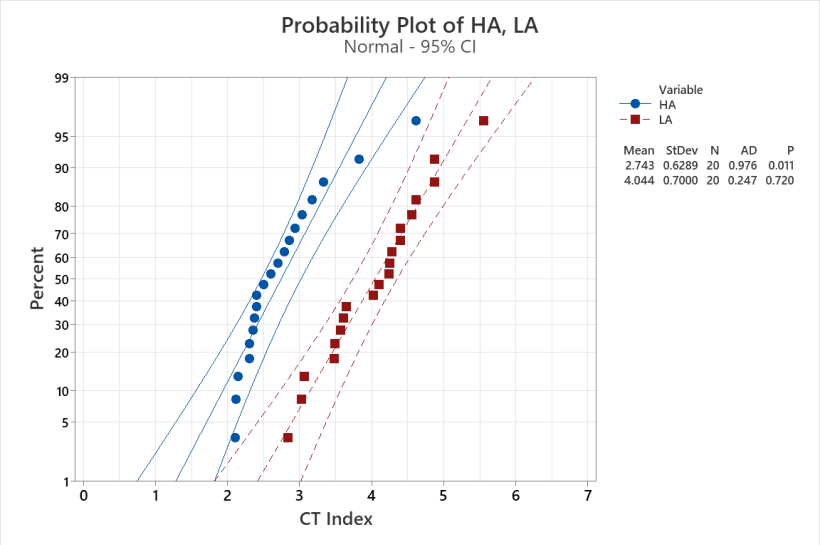

Figure 55. Probability Plot for Peak Load Comparison for Superpave Granite Mixes for both High and Low Angularities

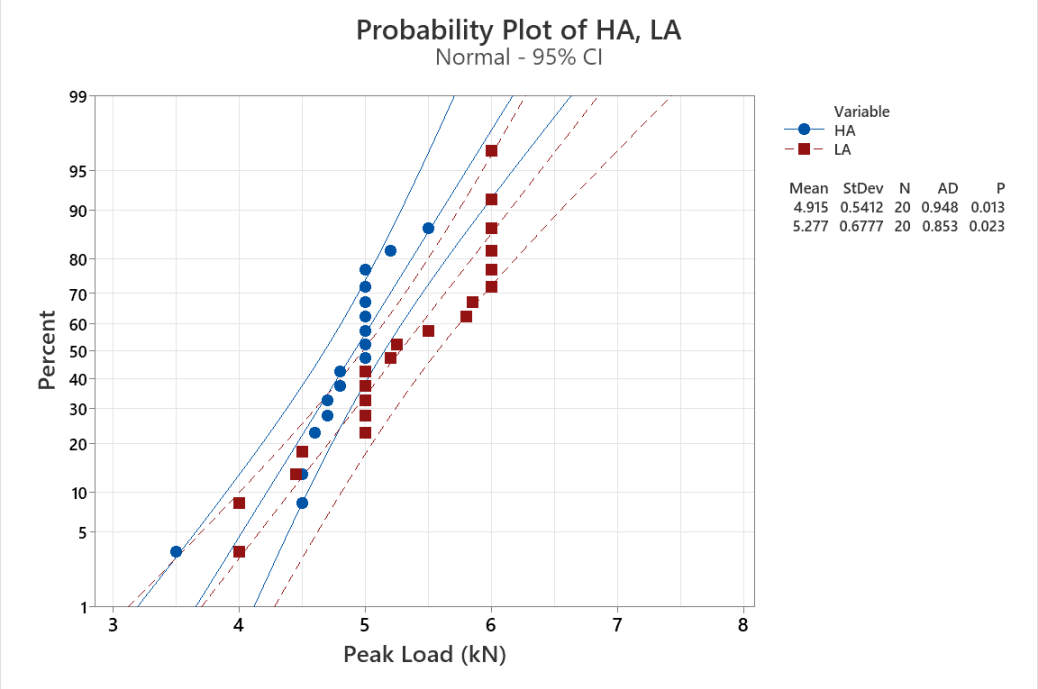

Figure 56. Probability Plot for CT Index Comparison for Superpave Granite Mixes for both High and Low Angularities

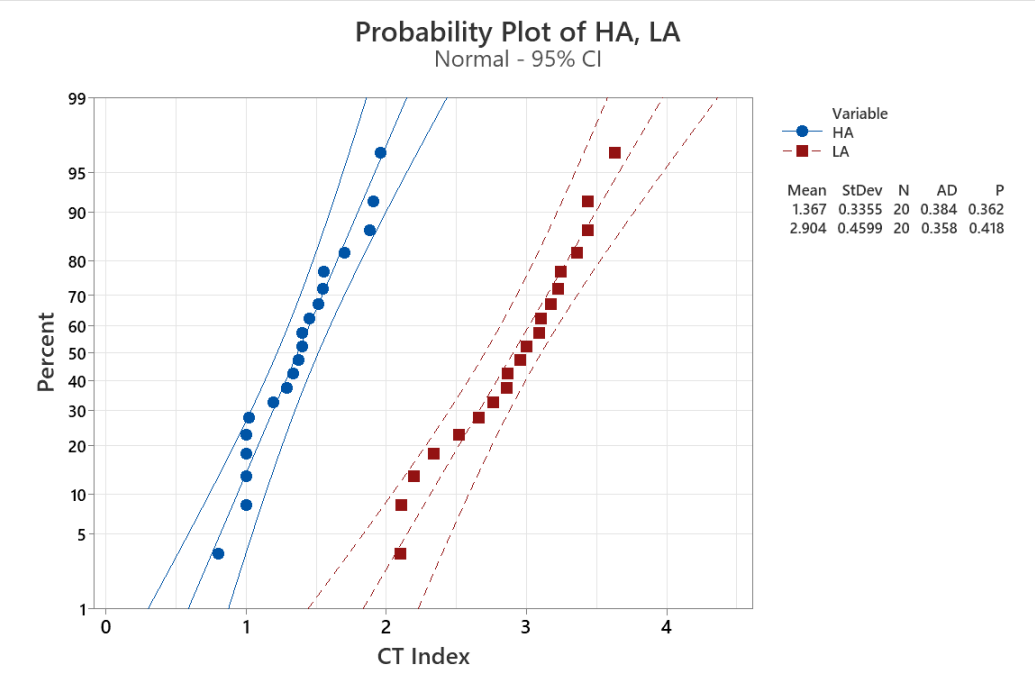

Figure 57. Probability Plot for Peak Load Comparison for Superpave HL Mixes for both High and Low Angularities

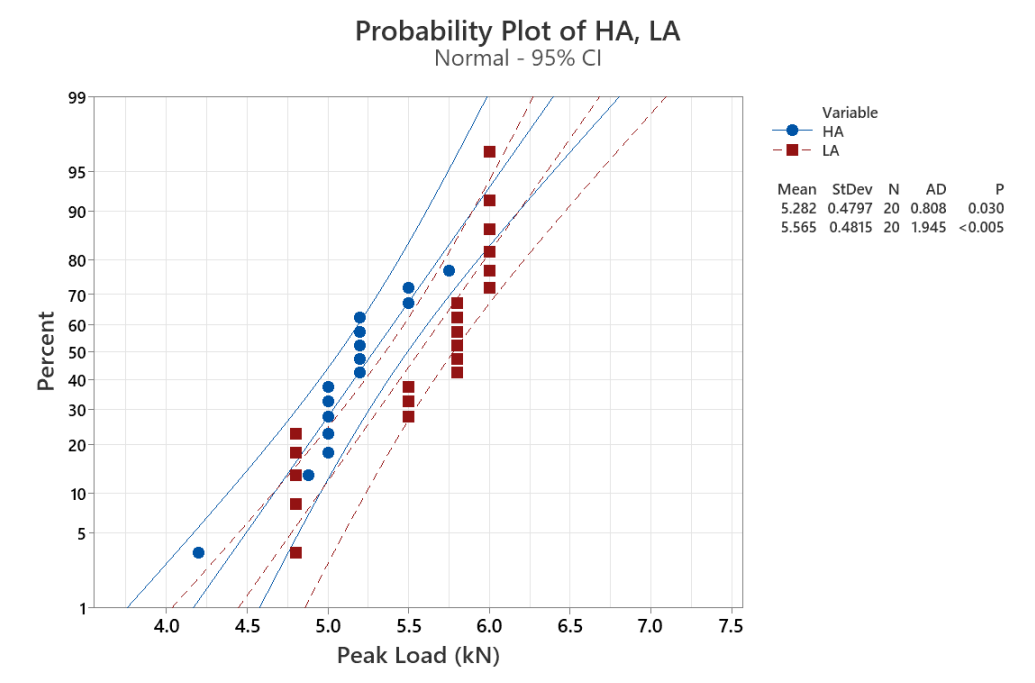

Figure 58. Probability Plot for CT Index Comparison for Superpave HL Mixes for both High and Low Angularities

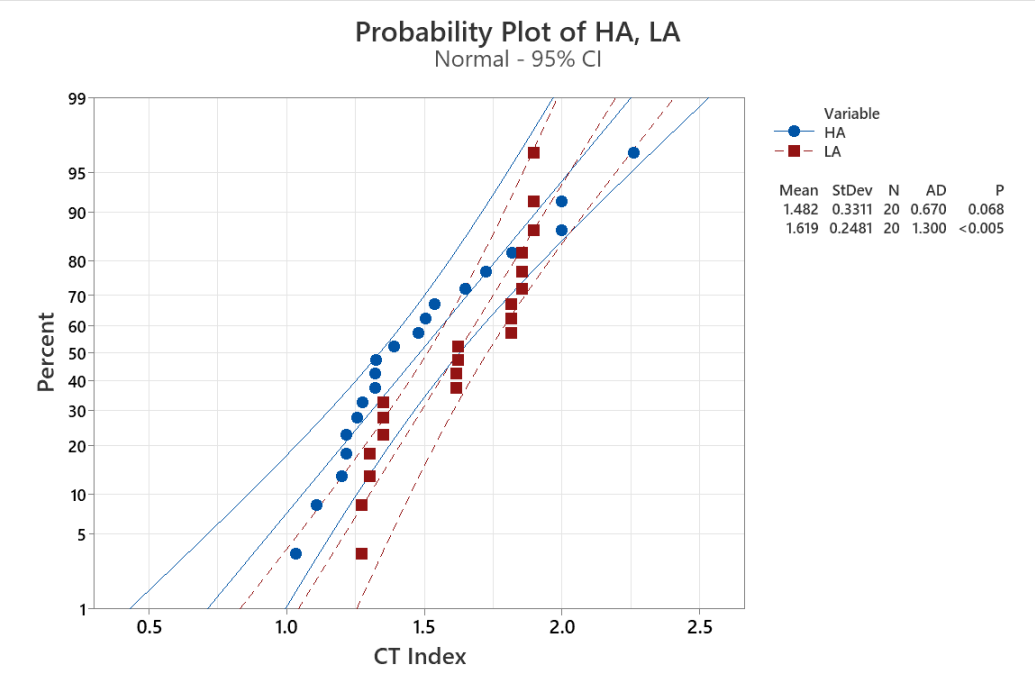

5.7 Angularities

The curves above mostly show that the peak load for whatever mix is in question will be greater for low angularity aggregate mixes than higher angularity aggregate mixes. The greatest difference is shown mostly for granite mixes where the peak load increases by 14% for CMHB mixes and 7% for Superpave mixes due to the lower percentage of aggregates in Superpave mixtures. Also, the peak load for hard limestone mixes increases slightly for low angularity aggregates. Therefore, low angularity aggregates can withstand a greater load than high angularity aggregates.

The CT index increases as well for low angularity aggregates, especially for granite mixes: increasing more than 40% for CMHB gradation and Superpave gradation. Also, the cracking resistance for hard limestone mixes increases for low angularity aggregates—it practically doubles the resistance for CMHB gradation and slightly increases the resistance for the Superpave gradation.

In summary, low angularity aggregates in a mix improve the overall cracking resistance of a sample and slightly increase the peak load it resists before failure. Even if these findings contradict the popular opinion of demanding high angularity aggregates for better resistance and stresses, they conform with the findings of previous studies where low angularity aggregates showed better cracking resistance on the asphalt pavement analyzer (APA test) in both laboratory tests and software simulations.

Table 18. Statistical Analysis of the Different Mixes

		Variable	Mean	STD Dev	COV (%)
CMHB-Granite	**HA**	Peak Load (KN)	3.91	0.54	13.94
		CT index	2.39	0.28	11.61
	LA	Peak Load (KN)	4.54	0.56	12.34
		CT index	4.15	0.96	23.04
CMHB-HL	**HA**	Peak Load (KN)	4.90	0.66	13.40
		CT index	2.74	0.60	21.80
	LA	Peak Load (KN)	4.94	0.57	11.49
		CT index	4.04	0.67	16.46
Superpave-Granite	**HA**	Peak Load (KN)	4.92	0.51	10.47
		CT index	1.37	0.32	23.34
	HL	Peak Load (KN)	5.28	0.64	12.22
		CT index	2.90	0.44	15.06
Superpave-HL	**HA**	Peak Load (KN)	5.28	0.46	8.64
		CT index	1.48	0.31	21.25
	HL	Peak Load (KN)	5.57	0.46	8.23
		CT index	1.62	0.24	14.57

The statistical analysis in the table above recapitulates the comparison procedure. First, the sample generation resulted in a coefficient of variation less than 30% for all sample calculations, so the tests conducted can be considered as repeatable, and the distribution of the 20 values for every simulation is uniformly distributed quite closely around the mean, which is indicated by a small standard deviation. Therefore, the average comparison (comparing means values) between mixes can accurately describe the whole series comparison (comparing the entire data sets). Hence, low angularity aggregates in a mix positively impact the cracking resistance of a mix. CMHB gradation has a better cracking resistance than Superpave gradation due to the increased percentage of aggregates, and between hard limestone and granite, granite has a weaker performance against cracking.

6. Summary and Conclusion

The IDEAL-CT tests conducted in this report were accomplished by running more than 400 simulations. The sensitivity study would require a great deal of time and material, so the distinct element method was implemented through PFC2D software to emulate the fracture behavior of a cylinder specimen under constant loading. Particle shapes were emulated in the software using the linear contact bond model in between particles. Properties of these modeled particles or aggregates, referred to as "bodies" in the simulation were deduced from previous calibration studies. Fracture distribution can be observed in the software, and the load displacement curves were exported for each simulation. The comparison study was solely based on these curves.

Aggregate images were drawn for the purpose of considering their shape or angularity in the variation, and two types of bonding material (hard limestone and granite) and two different gradation mixes (CMHB with greater aggregate percentage and Superpave) were taken into consideration. This variation was accompanied by a sensitivity study using two factors: air void content and loading rate. Based on these factors the following conclusions can be drawn:

- The IDEAL-CT test is sensitive to air void content, and it has a negative impact on the IDEAL-CT output.
- Even though an increase in loading rate yielded a poorer performance in cracking resistance and decreased peak load before breaking, the T-test showed that this increase is random, and that the loading rate does not have much of an impact on cracking resistance.
- CMHB gradation mixes perform better than Superpave mixes, hence mixes with a greater percentage of aggregates have better cracking resistance.
- Hard limestone can support greater peak loads prior to breaking and has slightly greater cracking resistance than granite based on the contact bond properties introduced.
- The angularity of the aggregates greatly impacts on cracking resistance. The lower the mix's angularity is, the better the cracking resistance will be, and the greater load a mix will support before failure.
- Sorting the variables by the most impactful to the least impactful yields the following: aggregate shape and angularity, mix gradation, and then material.
- Mix gradation and material type changes are introduced in the software through the values of the bonding strength of the particles.
- The IDEAL-CT test can be considered a repeatable cracking test based on its low coefficient of variation for every mix studied.

- The air void distribution in the sample dictates the trajectory of failure.
- Cracks mostly initiate underneath the loading bar and develop through air voids up until fractures connect and break the specimen.

7. Limitations and Future Work

This study's results are based on the experimental results gathered by previous studies and can be repeated for a new mix with different aggregate sizes and locations.

The following are suggestions for future testing:

- Two-dimensional models are used in this study in order to simplify calculations and analyses. However, this may not fully account for complexities of real-world applications. Hence, the same study could be done using three-dimensional modeling in the future, as it would offer more thorough understanding of the effects of aggregate variation, possibly such as depth, height, and more intricate spatial relationships that are difficult to assess in two-dimensional models.

- Temperature fluctuations, which could have a considerable impact on aggregate behavior, are not taken into account in this study. Introducing temperature as a variable can add another layer of realism to the model by seeing how aggregate sizes and positions are affected in various thermal environments.

References

[1]: ASTM D8225, 2019 Edition, April 1, 2019. (2019). "Standard Test Method for Determination of Cracking Tolerance Index of Asphalt Mixture Using the Indirect Tensile Cracking Test at Intermediate Temperature."

[2]: Saadeh, Shadi., Al-Zubi, Yazan, Mahmoud, Enad, Renteria, David, and Mohammad, Louay. (2020). "Sensitivity Analysis of Semi-Circular Bending Test using Plackett–Burman Matrix." *Transportation Research Record* 2674(2), 302–312. doi:10.1177/0361198120907587

[3]: Zhou, Fujie, Im, Soohyok, Sun, Lijun, and Scullion, Tom. (2017). "Development of an IDEAL cracking test for asphalt mix design and QC/QA." *Road Materials and Pavement Design* 18(4), 405–427. DOI: 10.1080/14680629.2017.1389082.

[4]: Han-Cheng, Dan, Zhang, Zhi, Chen, Jia-Qi, and Wang, Hao. (2018). "Numerical Simulation of an Indirect Tensile Test for Asphalt Mixtures Using Discrete Element Method Software." DOI: 10.1061/(ASCE)MT.1943–5533.0002252 © 2018 American Society of Civil Engineers.

[5]: Alvarado, Cesar, Mahmoud, Enad, Abdallah, lmad, Masad, Eyad, Nazarian, Soheil, Langford, Richard, Tandon, Vivek, Button, Joe. (2007). "Feasibility of Quantifying the Role of Coarse Aggregate Strength on Resistance to Load April2007 in HMA." Research Report 0–5268–1, *DOTF* 1700.7.

[6]: Monteiro Azevedo, Nuno, and Lemos, Jose Vieira. (2005). "Hybrid discrete element/finite element method for fracture analysis." *Computer Methods in Applied Mechanics and Engineering*, 195(33-36), 4579-4593. DOI: 10.1016/j.cma.2005.10.005

[7]: Abbas, Ala, Masad, Eyad, Papagiannakis, Tom, and Shenoy, Aroon. (2005). "Modelling asphalt mastic stiffness using discrete element analysis and micromechanics-based models." *International Journal of Pavement Engineering* 6(2), 137–146. DOI: 10.1080/10298430500159040.

[8]: Olsson, Erik, Jelagin, Denis, and Partl, Manfred N. (2019). "New discrete element framework for modelling asphalt compaction." *Road Materials and Pavement Design* 20(2), S604–S616. DOI: 10.1080/14680629.2019.1633750.

[9]: Kim, Yong-Rak and Souza, Leonardo T. "Effects of Aggregate Angularity on Mix Design Characteristics and Pavement Performance." (2009). *Final Reports and Technical Briefs from Mid-America Transportation Center* 25.

[10]: Zhou, Fujie, Im, Soohyok, Sun, Lijun, and Scullion, Tom. (2017). "Development of an IDEAL cracking test for asphalt mix design and QC/QA." *Road Materials and Pavement Design* 18(4), 405–427. DOI: 10.1080/14680629.2017.1389082.

[11]: Abbas, Ala, Papagiannakis, A.T., Masad, Eyad. (2006). "Micromechanical simulation of asphaltic materials using the discrete element method". *ASCE*.

[12]: Renteria, David, Mahmoud, Enad, ASCE, P.E., Yanez, Rolando, and Burbach, Victoria. (2017). "Discrete element analysis of SCB Variability-Asphalt mixture." *ASCE*.

About the Authors

Shadi Saadeh, PhD

Dr. Saadeh is a professor at California State University, Long Beach. He holds a Bachelor's Degree in Civil Engineering from the University of Jordan, a Master's Degree in Civil Engineering from Washington State University, and a PhD in Civil Engineering from Texas A&M University.

Maria El Asmar

Maria is currently a student of Master's in Civil Engineering at California State University, Long Beach. She holds a Bachelor's degree in Civil Engineering from Lebanese University Faculty of Engineering-II, Lebanon. Her research focuses on pavement material.

MTI FOUNDER

Hon. Norman Y. Mineta

MTI BOARD OF TRUSTEES

Directors